pubs.acs.org/Biomac

Article

SMALPs Are Not Simply Nanodiscs: The Polymer-to-Lipid Ratios of Fractionated SMALPs Underline Their Heterogeneous Nature

Elizabeth Kamilar, Jitender Bariwal, Wan Zheng, Hairong Ma, and Hongjun Liang*

Cite This: *Biomacromolecules* 2023, 24, 1819−1838

Read Online

ACCESS | Metrics & More | Article Recommendations | Supporting Information

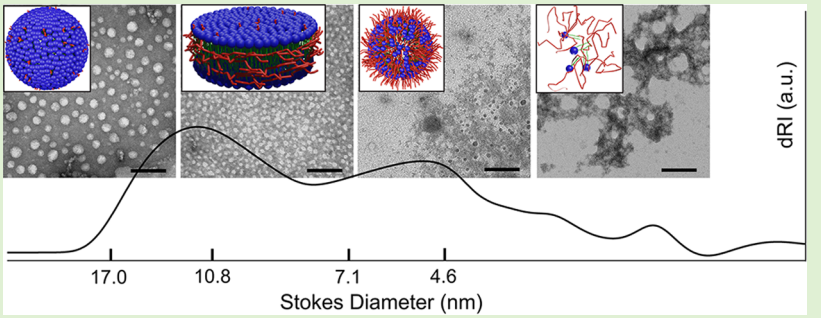

ABSTRACT: Amphipathic styrene-maleic acid (SMA) copolymers directly solubilize biomembranes into SMA-lipid particles, or SMALPs, that are often regarded as nanodiscs and hailed as a native membrane platform. The promising outlook of SMALPs inspires the discovery of many SMA-like copolymers that also solubilize biomembranes into putative nanodiscs, but a fundamental question remains on how much the SMALPs or SMALP analogues truly resemble the bilayer structure of nanodiscs. This unfortunate ambiguity undermines the utility of SMA or SMA-like copolymers in membrane biology because the structure and function of many membrane proteins depend critically on their surrounding matrices. Here, we report the structural heterogeneity of SMALPs revealed through fractionating SMALPs comprised of lipids and well-defined SMAs via size-exclusion chromatography followed by quantitative determination of the polymer-to-lipid (P/L) stoichiometric ratios in individual fractions. Through the lens of P/L stoichiometric ratios, different self-assembled polymer−lipid nanostructures are inferred, such as polymer-remodeled liposomes, polymer-encased nanodiscs, polymer−lipid mixed micelles, and lipid-doped polymer micellar aggregates. We attribute the structural heterogeneity of SMALPs to the microstructure variations amongst individual polymer chains that give rise to their polydisperse detergency. As an example, we demonstrate that SMAs with a similar S/MA ratio but different chain sizes participate preferentially in different polymer−lipid nanostructures. We further demonstrate that proteorhodopsin, a light-driven proton pump solubilized within the same SMALPs is distributed amongst different self-assembled nanostructures to display different photocycle kinetics. Our discovery challenges the native nanodisc notion of SMALPs or SMALP analogues and highlights the necessity to separate and identify the structurally dissimilar polymer−lipid particles in membrane biology studies.

INTRODUCTION

Self-assembled membranes such as liposomes, polymersomes, and supported planar membranes have made significant strides in applications ranging from drug delivery to biosensor design.[1−4] A self-assembled, free-standing two-dimensional (2D) membrane with controllable size at the nanoscale (i.e., nanodisc) could open new opportunities for technological innovations, but amphiphilic membranes by themselves do not normally assemble into nanodiscs due to the high energy cost to sustain the exposed hydrophobic membrane edge in aqueous solutions. Intriguingly, nanodisc exists and is deep-rooted in biology. It has long been known that lipids readily assemble into initially discoidal high-density lipoprotein nanoparticles with the help of human apolipoprotein A-1 (i.e., "apo A-1") to transport fat molecules and cholesterols from peripheral cells to the liver.[5] Sligar and colleagues were the first to show that recombinant apo A-1 termed membrane-scaffold proteins (MSPs) act as belts to encase lipid nanodiscs (LNDs) of adjustable diameters (i.e., ∼7−17 nm) in accordance with MSP sizes.[6,7] Despite being a newcomer to the self-assembled membrane family, LNDs have already made their marks on membrane biology,[8−10] therapeutics,[11−16] and clean energy and environment.[17−20]

From a polymer science point of view, MSPs are amphipathic random copolymers with monodisperse structures

Received: January 10, 2023
Revised: March 13, 2023
Published: March 22, 2023

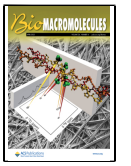

and uniform amphiphilic balances. The success of LNDs inspires long-lasting enthusiasm to explore both biotic[21−23] and abiotic[24−28] amphipathic membrane-scaffold polymers (MSPols) to support nanodiscs, but how to rationally design the structure of MSPols with the right amphiphilic balance to produce a hierarchy of inter- and intra-molecular forces with lipids in favor of their preferential co-assembly into nanodiscs rather than other forms of polymer−lipid nanostructures is not clear. The amphiphilic balance of amphipathic copolymers recapitulates their overall microstructures, such as hydrophobic/hydrophilic ratio, chain size, and sequence (i.e., block, alternating, statistical, or gradient). Tuning the amphiphilic balance to control the detergency and self-assembly behaviors of amphipathic copolymers is no stranger to polymer engineering. Polymer surfactants, or polysoaps, which have the amphiphilic balance resembling small detergents that solubilize biomembranes, have a long history of industrial applications ranging from emulsion stabilization to oil recovery.[29,30] Turning down their detergency, typically by scrambling the hydrophilic repeating units with the hydrophobic ones via random copolymerization, we obtain a big family of membrane-active polymers with intermediate detergency that translates into a wide spectrum of membrane-disrupting behaviors. Amphipols sit on one side of this spectrum (i.e., more detergency).[31,32] Given enough time, amphipols will rip biomembranes apart due to their fairly strong detergency,[33,34] although they are often used in membrane biology as surrogates to replace detergents bound to membrane proteins after the proteins are extracted and solubilized by the detergents from cell membranes first.[31,32] Biologically derived MSPs[6,35] would sit on the other side of this spectrum (i.e., less detergency); they have a fairly weak detergency that by itself is insufficient to solubilize biomembranes, but they can co-assemble with detergent-solubilized lipids into LNDs when the detergents are selectively removed. In-between amphipols and MSPs are two salient subgroups of copolymers known to create membrane defects or pores.[36,37] One subgroup is best known as membrane-active antimicrobial polymers as they kill bacteria by disrupting bacterial membranes;[38,39] the other subgroup, which includes SMA and SMA-like copolymers, are sometimes called hypercoiling polymers as they exhibit pH- or temperature-triggered shift of amphiphilic balance with ensued conformational change to breach biomembranes, a trait that is highly valued for stimuli-responsive drug delivery.[40−44] Interestingly, examples of MSPols that directly solubilize biomembranes into LNDs have been reported from both subgroups of copolymers,[24,27] underscoring the versatility of tuning the amphiphilic balance and detergency of synthetic copolymers to serve as MSPols.

In contrast to biologically derived MSPs with monodisperse structures and uniform amphiphilic balances, synthetic polymers are inherently heterogeneous. It would be unrealistic to assume that all polymer chains reach the delicate amphiphilic balance just enough to solubilize biomembranes into nanodiscs without venturing into other forms of self-assembled polymer−lipid nanostructures. Nevertheless, since the early report of SMALPs[24] in 2009, there has been a gradual shift of interpretation toward simply equating SMALPs or SMALP analogues to LNDs,[45−53] oftentimes one step further to native nanodiscs.[54−58] Although the important effect of amphiphilic balance, such as the *S*/MA ratio[59−63] and chain size[63−66] on SMALP formation, has been well documented, very few studies exist to quantitatively analyze the compositional and structural heterogeneity of SMALPs or SMALP analogues, with only recent reports starting to question the native nanodisc notion by lipidomic[67] and small-angle X-ray scattering (SAXS) analysis.[68]

One possible reason for the simplified interpretation of SMALPs or SMALP analogues as LNDs is the technical challenge of discerning nanodiscs from other forms of polymer−lipid nanostructures; this challenge is likely exacerbated by the heterogeneous nature of SMALPs or SMALP analogues themselves. For classical LNDs encased by MSPs, the formation of LNDs was explicitly confirmed by a set of complementary probes, including size-exclusion chromatography (SEC) (i.e., a single eluted fraction within the expected size range), atomic force microscopy (AFM) (i.e., asymmetric disc-like structures with a uniform diameter greater than their thickness as expected from a lipid bilayer), SAXS (i.e., the unique scattering profile characteristic of LNDs showing a sharp minimum and a broad maximum, from which the pair distribution function can be computed to confirm the thickness and radius of gyration of the LNDs, respectively), and last but not the least important, quantitative determination of the number of MSPs and MSP-to-lipid stoichiometric ratio in individual LNDs, which helped indisputably establish the nanodisc model by correlating the diameter of LNDs with the length of MSP and the total number of lipids per LND based on simple geometric considerations.[6,7] This level of clarity is lacking when SMALPs or SMALP analogues were conjectured as LNDs or native nanodisc,[24−28,44−61,63−66] where characterization tools such as transmission electron microscopy (TEM), dynamic light scattering (DLS), differential scanning calorimetry (DSC), and nuclear magnetic resonance (NMR) spectroscopy were frequently relied upon instead. While all of those methods are powerful in revealing the transition from liposomes to polymer-solubilized membranes, none of them can tell whether the resulting polymer−lipid particles truly resemble the bilayer structure of nanodiscs. For example, TEM aided by negative staining to enhance contrast usually cannot tell the difference between spherical micelles, liposomes, and LNDs, nor the difference between cylindrical micelles and "edge-on" LNDs. TEM tomography reconstructed from a series of images taken at systematically varied tilting angles under preferentially cryogenic conditions to minimize artifacts induced by radiation damages will help, but such studies have not been reported yet. DLS shows the downsizing process when liposomes are solubilized by the copolymers, but it does not tell whether the downsized products are LNDs. DSC reveals the change of lipid transition temperature when liposome membranes are disrupted, but it too does not tell whether the disrupted liposomes become LNDs. The magnetic alignment, chemical shift, and peak width in ^{31}P-NMR spectroscopy reflect the transition from large, isotropic, and slow-tumbling phospholipid vesicles to disrupted, anisotropic polymer-remodeled liposomes and smaller, fast-tumbling polymer−lipid nanoparticles, but those changes are unable to tell whether the disrupted and dismantled vesicles become LNDs.

To further cast a shadow on the LND or native nanodisc notion of SMALPs or SMALP analogues, small-angle scattering studies of the polymer-solubilized membranes have not revealed the characteristic nanodisc scattering profile similar to that observed for LNDs.[7] Although the neutron scattering feature of SMALPs was fit by a polymer-encased nanodisc

https://doi.org/10.1021/acs.biomac.3c00034
Biomacromolecules 2023, 24, 1819−1838

model in an early study,[69] a recent study used this simple LND model to fit the single broad SAXS peak but failed.[68] Additionally, lipidomic analysis has confirmed that the lipid compositions of SMALPs or SMALP analogues produced by different copolymers differ from that of the native membranes as well as from each other,[67] suggesting that biomembranes are disrupted and solubilized by the structurally dissimilar SMAs or SMA-like copolymers in different manners, possibly due to their different amphiphilic balances. Furthermore, the lipid-to-protein ratios of solubilized membrane proteins in SMALPs or SMALP analogues were determined on a few occasions, but none of the ratios are consistent with a simple LND model. For example, the lipid-to-bacteriorhodopsin ratio in SMALPs was measured to be 10.7 ± 0.7,[24] and the lipid-to-rhomboid protease ratio in diisobutylene-maleic acid lipid particles (DIBMAPs) was measured to be 10.[45] Both ratios are one order of magnitude lower than that expected from a membrane protein-carrying LND of a similar size (i.e., ∼100, assuming that half of the LND space is occupied by the protein),[7,8] but rather resemble the number of lipids closely bound to individual membrane proteins as revealed in the crystallographic studies of detergent-solubilized bacteriorhodopsin (i.e., 9)[70] and rhomboid protease (i.e., 14),[71] respectively, suggesting the possibility that a significant portion of membrane proteins solubilized by SMALPs or DIBMAPs might reside in polymer micelles instead of LNDs.

Clearly, despite the rapid development of SMALPs or SMALP analogues for use in membrane biology, a fundamental question remains on how much those polymer-solubilized membranes truly resemble the bilayer structure of LNDs. Blurring the difference between the two is detrimental because it not only confuses data interpretation (for example, structural and functional analysis of membrane proteins would be different if their heterogeneous surrounding matrices are taken into account) but also ignores the more important question, i.e., how to rationally design MSPols that would preferentially cut lipid bilayers into LNDs instead of solubilizing them into micelles?

To shed light on the structural heterogeneity of SMALPs or SMALP analogues and illuminate the guiding concepts on the rational design of MSPols with the right amphiphilic balance in favor of LND formation, we quantitatively determined the polymer-to-lipid (P/L) stoichiometric ratios in fractionated SMALPs comprised of a model lipid and well-defined SMA. Like the MSP-to-lipid ratio that played a critical role in validating the nanodisc model of LNDs,[6,7] the P/L stoichiometric ratio is a fundamental parameter critical to unravel the complex structures of SMALPs or SMALP analogues. Unfortunately, this ratio has remained elusive until now, partly because the copolymers used in most studies of SMALPs or SMALP analogues have broad distributions of chain sizes. We used reversible addition−fragmentation chain transfer (RAFT) polymerization to synthesize SMAs with well-defined chain sizes as a model system and SEC to separate the different SMALP components by sizes. Through the lens of P/L stoichiometric ratios, we identified a series of self-assembled SMALP structures such as polymer-remodeled liposomes, polymer-encased nanodiscs, polymer−lipid mixed micelles, and lipid-doped polymer micellar aggregates, and further verified the structural heterogeneity of SMALPs using an array of complementary characterization tools such as TEM, DLS, DSC, and ^{31}P-NMR. We attribute the structural diversity of SMALPs to the microstructure variations of individual polymer chains that give rise to their polydisperse detergency. As an example, we demonstrated that well-defined SMAs with a similar S/MA ratio but different chain sizes show vastly different preferences in participating in the different polymer−lipid nanostructures. Furthermore, we demonstrated that proteorhodopsin, a light-driven proton pump, solubilized within the same SMALPs is distributed amongst different polymer−lipid nanostructures to display different photocycle kinetics. Our discovery challenges the native nanodisc notion of SMALPs or SMALP analogues and highlights the necessity to separate and identify the structurally dissimilar polymer−lipid particles in membrane biology studies.

MATERIALS AND METHODS

Materials. Styrene (inhibited with ∼0.005% 4-*tert*-butylcatechol) and maleic anhydride (puriss p.a., ACS reagent, ≥99.0%) were purchased from Sigma-Aldrich (St. Louis, MO). Before styrene was used in polymerization, the inhibitor was removed by passing the monomer through a basic aluminum oxide column. Azobisisobutyronitrile (AIBN) (98%, Sigma-Aldrich) was recrystallized from ethanol twice before use. *S*-1-Dodecyl-S′-(α,α'-dimethyl-α''-acetic acid) trithiocarbonate (DATC) was synthesized according to the literature.[72] The commercially available styrene and maleic anhydride random copolymer (hereafter referred to as "SMAnh"), i.e., the Lipodisq SMAnh (S/MA ∼ 2/1), was gifted from Malvern Cosmeceutics (WR14 3SZ, United Kingdom) and used as control. It has a weight-average ($\overline{M_w}$) and number-average molecular weight ($\overline{M_n}$) of 7.5 and 2.8 kDa, respectively, with a polydispersity index ($Đ$) ∼ 2.68, as reported by Malvern Cosmeceutics. Alexa Fluor 647 C_2 maleimide (AF647) was purchased from Thermo Fisher Scientific Inc. (Waltham, MA). 1,2-Dimyristoyl-*sn*-glycero-3-phosphocholine (DMPC) and fluorescent 1,2-dimyristoyl-*sn*-glycero-3-phosphoethanolamine-*N*-(7-nitro-2-1,3-benzoxadiazol-4-yl) (ammonium salt) (NBD-PE) were purchased from Avanti Polar Lipids (Birmingham, AL). *n*-Dodecyl-β-D-maltoside (DDM, ≥99.0%) was purchased from Anatrace Products, LLC. (Maumee, OH). The expression and purification of proteorhodopsin (PR; BAC31A08 with a 6× His tag) were described in our previous report.[25] All other chemicals were purchased from Sigma-Aldrich at reagent grade or higher when available and used as received unless otherwise specified.

Synthesis of Well-Defined SMAnh by RAFT Polymerization. Three model SMAnh copolymers with a similar S/MA ratio but different molecular weights were synthesized. The polymerization protocol is adapted from our previous report[73] but with a few modifications (Scheme S1a, Supporting Information (SI)). In a typical run to prepare SMAnh with a S/MA of ∼ 2/1 and a molecular weight of $\overline{M_n}$ ∼ 6 kDa, styrene (5.46 g, 52.5 mmol), maleic anhydride (735 mg, 7.5 mmol), DATC (72.8 mg, 0.2 mmol), and AIBN (3.28 mg, 0.02 mmol) were dissolved in 5.5 mL inhibitor-free tetrahydrofuran (THF) in a 25 ml Schlenk flask, stirred, and degassed by three freeze−pump−thaw cycles. The flask was then sealed and immersed in an oil bath kept at 70 °C. The polymerization was run for a predetermined time (∼140 min) obtained from the kinetics study[74] to reach a conversion of ∼20%. The reaction mixture was then quenched by liquid nitrogen and precipitated three times with an excess of ether/chloroform (3:1 v/v). The polymer product was collected by centrifugation, dried in a vacuum, weighed, and characterized by ^{1}H NMR and SEC.

In a typical run to prepare SMAnh with a S/MA of ∼ 2/1 and a molecular weight of $\overline{M_n}$ ∼ 3 kDa, styrene (2.674 g, 25.7 mmol), maleic anhydride (420.0 mg, 4.3 mmol), DATC (72.8 mg, 0.2 mmol), and AIBN (6.5 mg, 0.04 mmol) were dissolved in 7.0 mL of inhibitor-free THF in a 25 mL Schlenk flask, stirred, and degassed by three freeze−pump−thaw cycles. The flask was sealed and immersed in an oil bath kept at 70 °C. The polymerization was run for a predetermined time (∼95 min) to reach ∼20% conversion. The

https://doi.org/10.1021/acs.biomac.3c00034
Biomacromolecules 2023, 24, 1819−1838

reaction mixture was then quenched, and the polymer product was recovered and characterized similarly as discussed above.

In a typical run to prepare SMAnh with a S/MA of ∼ 2/1 and a molecular weight of $\overline{M_n}$ ∼ 12 kDa, styrene (5.546 g, 53.3 mmol), maleic anhydride (653.3 mg, 6.7 mmol), DATC (36.4 mg, 0.1 mmol), and AIBN (3.4 mg, 0.02 mmol) were dissolved in 5.5 mL of inhibitor-free THF in a 25 mL Schlenk flask, stirred, and degassed by three freeze−pump−thaw cycles. The flask was sealed and immersed in an oil bath kept at 70 °C. The polymerization was run for a predetermined time (∼120 min) to reach ∼20% conversion. The reaction mixture was then quenched, and the polymer product was recovered and characterized similarly as discussed above.

Synthesis of SMA and Fluorescently Labeled SMA. The SMAnh synthesized by RAFT polymerization (i.e., "RAFT SMAnh") was hydrolyzed under mild conditions in triethylamine (TEA) solution to preserve the terminal trithiocarbonate moiety as reported before[63] with minor changes (Scheme S1b, SI), and the Lipodisq SMAnh control was hydrolyzed in NaOH solution. In a typical run, the RAFT SMAnh (500 mg) was added into a mixture of THF (5 mL), Millipore water (3 mL), and TEA (1 mL) in a round bottom flask. The flask was placed in an oil bath kept at 70 °C to react for 60 min. Dilute HCl solution was then added into the reaction mixture to drop the pH to ∼5, and the clear solution was transferred into a SpectraPor dialysis bag (MWCO = 1 kDa) (Repligen Corp., Waltham, MA) and dialyzed against Millipore water for 2 days to completely remove the organic solvent and TEA-salt, followed by lyophilization to obtain a yellowish white polymer. The hydrolysis of Lipodisq SMAnh control was performed similarly, except that 10 mL of 1 M NaOH was used in place of the THF/water/TEA mixture. The final SMA products were characterized by ^{1}H-NMR and Fourier transform infrared (FT-IR) to confirm the complete hydrolysis.

To prepare fluorescently labeled SMA-AF647, the terminal trithiocarbonate moiety on the SMA derived from RAFT SMAnh was first converted to a thiol moiety (Scheme S1c, SI). In a typical run, the SMA was dissolved in a mixture of *N*,*N*-dimethylformamide (DMF)/water (1:1). Butylamine (∼5 equivalency to SMA) was added, and the reaction mixture was stirred at room temperature for 24 h under N_2 protection, then transferred into a SpectraPor dialysis bag (MWCO = 1 kDa) to dialyze against Millipore water for 3 days, followed by lyophilization to obtain the SMA-SH as a white powder. Next, the SMA-SH was dissolved in a mixture (1:1) of dimethyl sulfoxide (DMSO) and an aqueous solution of 10 mM tris(2-carboxyethyl)phosphine (TCEP). The reaction mixture was stirred for 3 h at room temperature under N_2 protection and then added in a stock solution of AF647 (in DMSO) at ∼0.5% equivalency to the SMA-SH. The reaction mixture was stirred at room temperature overnight under N_2 and light protection to conjugate AF647 to SMA via the thiol-maleimide click reaction, followed by dialysis against Millipore water in a SpectraPor dialysis bag (MWCO = 2 kDa) and lyophilization (both under light protection) to give a light blueish polymer. The successful conjugation of AF647 was confirmed by fluorescence spectroscopy.

Preparation of SMALPs. Small unilamellar vesicles of DMPC were prepared as reported previously[75] in a Tris buffer (10 mM Tris, 20 mM NaCl, pH 7.4) at desired concentrations (e.g., 10 mg/mL), and SMAs were dissolved separately in Tris buffer at desired concentrations (e.g., 10 mg/mL). SMALP formation was initiated by mixing stock solutions of SMA and DMPC at different *P*/*L* weight ratios. For comparison of SMALPs at different *P*/*L* weight ratios, the total volume and total weight of polymer plus lipid, respectively, in each sample were kept the same, such that the concentration of the total self-assembly components in each sample is identical. For instance, suppose each SMALP sample has a total volume of 1 mL, and both lipid and polymer stock solutions have the same concentration (e.g., 10 mg/mL), we would mix 0.5 mL of lipid and 0.5 mL of polymer stock solutions to prepare SMALPs at a *P*/*L* weight ratio of 1/1, and mix 0.25 mL of lipid and 0.75 mL of polymer stock solutions to prepare SMALPs at a *P*/*L* weight ratio of 3/1, and so on and so forth. The mixture was vortexed for 5 min, followed by incubation at 37 °C overnight, during which the initially turbid solution became clear.

Preparation of PR-Carrying SMALPs. PR-carrying proteoliposomes were first prepared following the classic detergent-assisted reconstitution protocol[76] with modifications optimized for the PR-DMPC system. Specifically, proteoliposomes were prepared first by mixing DDM-solubilized PR, DMPC (DMPC-to-PR stoichiometric ratio of ∼ 250:1), and DDM (final concentration of ∼2.47% (w/v)) in the prep buffer (20 mM Tris, 0.1 M NaCl, 0.5 mM EDTA, 0.01% NaN_3, pH = 7.4). We tested a few DDM concentrations, and this concentration was chosen because it is the lowest DDM concentration that still allows complete solubilization of DMPC liposomes, as revealed by DLS studies. The sample was incubated with gentle stirring at room temperature overnight. It was then diluted 10 times by dropwise addition of the prep buffer and dialyzed against the prep buffer, against the prep buffer diluted by Millipore water (1:1 dilution), and finally against the Tris buffer (10 mM Tris, 20 mM NaCl, pH 7.4). The final sample was concentrated using 10 kDa Amicon centrifuge filters (MilliporeSigma, Burlington, MA), then washed three times with Tris buffer (10× volume) and concentrated again using the 10 kDa centrifuge filters. The final triple washes were performed to ensure the removal of residual DDM, if there is any, as much as possible. The PR-carrying SMALPS were prepared via solubilization of the proteoliposomes by SMAs at a *P*/*L* = 3/1 weight ratio, with gentle stirring overnight at room temperature.

SEC. Characterization of SMALPs and separation of different SMALP components were performed in the Tris buffer on an Agilent 1260 Infinity II Bio-Inert HPLC system consisting of a quaternary pump, a multiple wavelength diode array UV-Vis detector, a thermostatted column compartment, a fraction collector, a universal interface box, and a manual FL-injection valve (Agilent Technologies, Inc., Santa Clara, CA). The system is further integrated with a Wyatt Optilab REX refractive index (RI) detector, a miniDAWN TREOS multiangle light scattering (MALS) detector, and a Wyatt ViscoStar III viscometer (Wyatt Technology Corp., Santa Barbara, CA). A Superdex 200 10/300 GL column (GE Healthcare, Marlborough, MA) was used as the separation column, and the Tris buffer (10 mM Tris, 20 mM NaCl, pH 7.4) was used as the eluent running at a flow rate of 0.5 mL/min. SEC runs were performed with either 20 or 500 μL injection for size characterization or fraction collection, respectively. All samples were filtered through a 200 nm Whatman Nylon filter prior to injections.

For a subset of regular SMALPs, fluorescently labeled SMALPs, and PR-carrying SMALPs, respectively, individual fractions of SMALPs after passing the SEC column were collected. Specifically, 500 μL of SMALPs at 40 mg/mL was injected into the Agilent 1260 system equipped with the Superdex 200 10/300 GL column, and the SEC fractions in the Tris buffer were collected for each 0.5 mL elution volume. The same SEC run was repeated 5−10 times, and the fractions of the same elution volumes in all runs were combined to collect sufficient samples for the specific experiment that followed.

All model SMAnh were also characterized by the Agilent 1260 system. A Waters Styragel HR 4E column (Waters, Milford, MA) incubated at 60 °C was used as the separation column, the RI detector was used as the concentration detector, and HPLC-grade DMF containing 0.01% (v/w) LiBr was used as the eluent running at a flow rate of 0.5 mL/min. Data were processed with the Wyatt ASTRA (version 7.3.2.19) to obtain the $\overline{M_n}$, $Đ$ (from the MALS detector), and viscosity-average molecular weight $\overline{M_v}$ (from the viscometer), respectively.

Characterization of SMA in Different SMALP Fractions. To test the possibility that SMA of different amphiphilic balances may contribute differently to the formation of the different SMALP components, individual SEC fractions of SMALPs consisting of DMPC and a 1:1 mixture (weight ratio) of SMA copolymers with a similar S/MA ratio but two different chain lengths were collected as described above. The pooled fractions were lyophilized and redissolved in 0.2 mL of HPLC-grade DMF (with 0.01% (v/w) LiBr), then characterized by the Agilent 1260 system equipped with

https://doi.org/10.1021/acs.biomac.3c00034
Biomacromolecules 2023, 24, 1819−1838

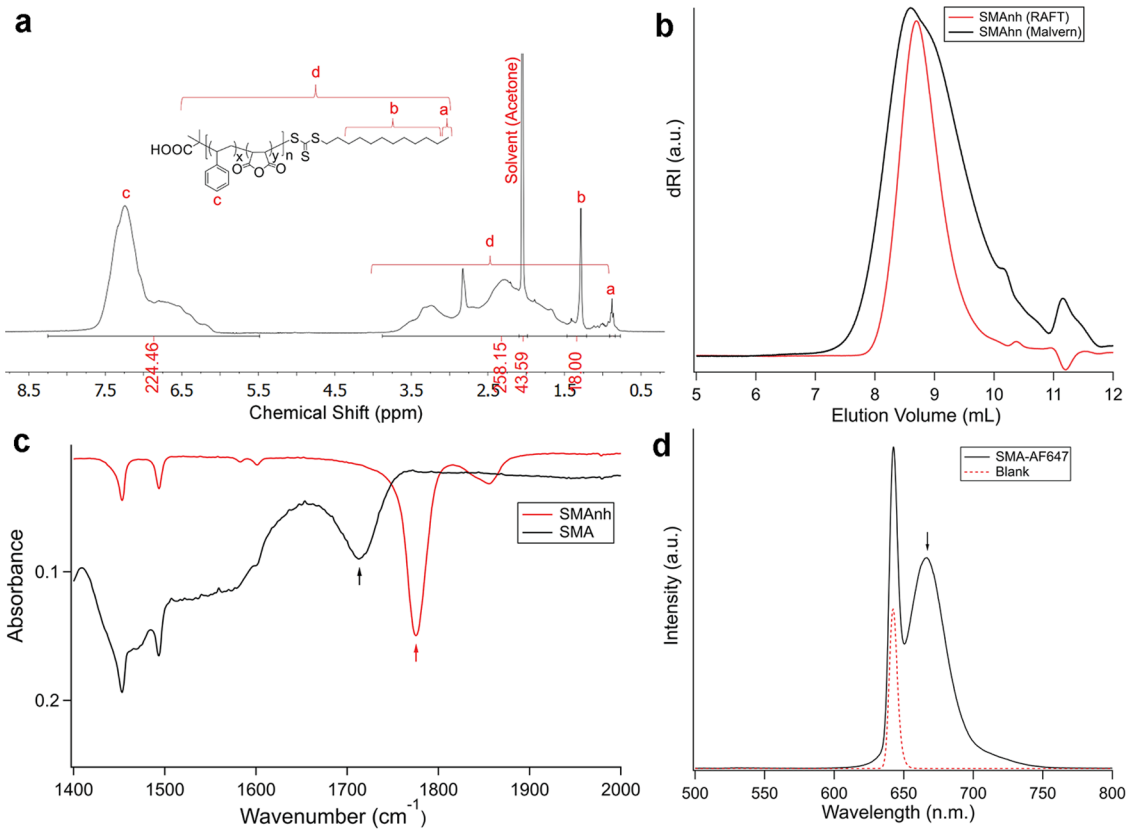

Figure 1. Characterization of model SMA copolymers. (a) The ^{1}H-NMR spectrum of RAFT SMAnh-*m*. The chemical shifts of different aromatic and alkyl protons on SMAnh (inset) are assigned, and peak integration using 18-H on the DATC moiety (marked as *b*) as the internal standard suggests that this SMAnh consists of 45 styrene and 24 maleic anhydride units. (b) SEC elution profiles of RAFT SMAnh-*m* (red trace, $Đ \sim 1.05$) and Lipodisq SMAnh (black trace, $Đ \sim 2.57$). (c) FT-IR spectra of RAFT SMAnh-*m* before (red trace) and after hydrolysis (black trace), with their carbonyl stretching peak absorbance marked by an arrow. (d) Fluorescence spectroscopy of SMA-AF647 (black trace) as compared to the SMA-SH control (red trace) that only shows the excitation wavelength at 640 nm. The peak emission of SMA-AF647 is marked by an arrow.

the Waters Styragel HR 4E column running HPLC-grade DMF (with 0.01% (v/w) LiBr) as the eluent at a flow rate of 0.5 mL/min. As controls, individual SMA copolymers and their 1:1 mixture (weight ratio), respectively, were also characterized by the Agilent 1260 system under the same configuration. Test runs of DMPC and Tris residues by themselves under the same SEC configurations confirmed that they did not interfere with the SMA elution peaks.

Since the RI detector is a concentration detector, quantitative analysis of the distribution of the two SMA copolymers in different SMALP fractions was performed via analysis of the RI signals contributed by individual SMA copolymers. Specifically, the elution peaks of the two SMA copolymers by themselves, monitored by the RI detector, were fit using the exponentially modified Gaussian (EMG) functions. The two copolymer EMG functions were then used to fit the elution peaks of all SMALP fractions to obtain the percentage contributions from each SMA copolymer in individual SMALP fractions. All peak fittings were performed using Igor Pro (version 7.08) from WaveMetrics, Inc. (Lake Oswego, OR). The utility of this method was confirmed by fitting the elution peak of the 1:1 SMA copolymer mixture, in which a ∼50% contribution from each SMA copolymer was obtained.

Quantification of DMPC and SMA. Quantification of DMPC and SMA in individual SMALP fractions was achieved by monitoring the fluorescently labeled SMALPs consisting of DMPC (doped with ∼0.5% NBD-PE; ex/em = 460/535 nm) and SMA (doped with ∼0.5% SMA-AF647; ex/em = 650/665 nm) on a Hitachi F-7000 Fluorescence Spectrophotometer (Hitachi High-Tech America, Inc., Dallas, TX) connected to a Fischer Scientific Isotemp 3016S Water Cooling Pump. The calibration curves of fluorescently labeled DMPC and SMA by themselves were established using their emission peaks centered at 535 and 665 nm, respectively (Figure S5, SI). SMALP fractions were collected under light protection from multiple SEC runs, as described earlier. Individual fractions were lyophilized and rehydrated in 0.2 mL of Millipore water under light protection prior to fluorescence studies. Each sample was measured in triplicate, and an average emission intensity was determined by the data processing package FL Solutions (version 4.2).

Characterization of the Photocycle Kinetics of PR by Flash Photolysis. The proton-pumping photocycle of PR was characterized by a series of spectroscopically distinctive intermediate states. Flash photolysis experiments were performed to compare the PR-mediated proton-pumping kinetics when PR was embedded in different surrounding matrices: (i) proteoliposomes, (ii) detergent micelles (i.e., DDM-solubilized proteoliposomes), and (iii) SMALPs (i.e., proteoliposomes solubilized by RAFT SMA-*m*). For (ii) and (iii), the same proteoliposomes in (i) consisting of PR and DMPC were used. The SMALP fractions of different sizes were collected as described earlier. All samples were buffer exchanged to the Tris buffer adjusted to pH = 9 before measurements.

The custom-built photolysis system consists of four major components, a Continuum Minilite II Q-switched Nd:YAG pump laser (Continuum Electro-Optics Inc., Milpitas, CA), a probe LED light (Thorlabs, Newton, NJ), a PMT detector (Hamamatsu, Shizuoka, Japan), and a PC oscilloscope (Pico Technology, Tyler, TX). High-energy (mJ) nanosecond-duration laser pulses at 532 nm were generated from the pump laser, first vertically focused before reaching the sample and then spatially overlapped with the probe beam at the sample center. Flash photolysis of the PR sample was produced by laser light absorption, leading to transient absorption changes due to the formation and decay of various photocycle intermediate states during the consecutive photochemical events. We

https://doi.org/10.1021/acs.biomac.3c00034
Biomacromolecules 2023, 24, 1819−1838

selected two characteristic wavelengths at 500 and 600 nm that reflect the overall photocycle turnover kinetics and the retinal isomerization kinetics, respectively, to report the photocycle kinetics of PR, as we reported before.[77] The raw data were loaded into Igor Pro, averaged, and analyzed to compare the kinetics of PR embedded in different matrices.

NMR. The NMR spectra were measured on a JEOL ECS 400 MHz spectrometer (JEOL USA, Inc., Peabody, MA), and data analysis was performed using MestReNova (version 11.0; Mestrelab Research S.L., Escondido, CA). ^{1}H-NMR spectra of RAFT SMAnh were collected with acetone-d_6 as the solvent. To determine the average degree of polymerization (DP) of styrene and maleic anhydride units as well as the S/MA ratio in RAFT SMAnh, the 18 protons in the hydrocarbon tail of the DATC moiety (δ = 1.20−1.47 ppm) at the end of each polymer chain were used as the internal reference (Figure 1a), from which the total aromatic protons (A_s) from the styrene repeating units in the range of δ = 6.0−8.0 ppm, and the total alkyl protons (A_a) in the range of δ = 0.5−4.0 ppm that include contributions from the polymer backbone (A_{pol}), acetone solvent (A_{sol}), and the chain transfer agent (CTA) moiety (A_{cta}, 31 for DATC) were determined. The average DP of styrene repeating units (DP_S) was calculated as $DP_S = A_s/5$, and the average DP of maleic anhydride repeating units (DP_{MA}) was calculated as $DP_{MA} = (A_a - A_{sol} - A_{cta} - 3 \times DP_S)/2$, as each styrene and maleic anhydride repeating unit contributes 3 and 2 alkyl protons to the polymer backbone, respectively. The S/MA ratio was calculated as $S/MA = DP_S/DP_{MA}$, and the molecular weight of the SMAnh was calculated as $\overline{M_n} = 104 \times DP_S + 98 \times DP_{MA} + 364$, where 104, 98, and 364 are the molecular weight of the styrene, maleic anhydride, and DATC, respectively.

To confirm the utility of NMR analysis in determining the S/MA ratios, we also collected the ^{1}H-NMR spectrum (in Acetone-d_6) of Lipodisq SMAnh and determined its S/MA ratio. The peak areas of all aromatic (A_s) and alkyl protons (A_a) in the range of δ = 6.0−8.0 ppm and δ = 0.5−4.0 ppm, respectively, were integrated in relative scale. The peak area of alkyl protons from the polymer backbone was calculated as $A_{pol} = A_a - A_{sol}$ and the S/MA ratio was calculated as $S/MA = DP_S/DP_{MA} = 2 \times A_s/(5 \times A_{pol} - 3 \times A_s)$. The S/MA ratio of the Lipodisq SMAnh was determined to be ∼1.9 via NMR analysis (Figure S1, SI), which is very close to the number (i.e., ∼2) provided by Malvern Cosmeceutics.

^{31}P-NMR spectra of DMPC in SMALPs dissolved in Tris buffer doped with 10% D_2O were collected at 30 °C. SMALP samples were prepared with different P/L weight ratios but the same amount of DMPC. The integrated area of the ^{31}P peak in each SMALP sample was normalized by the one that has the largest ^{31}P peak area.

DSC. The gel-to-liquid crystalline transition temperature of DMPC in liposomes, detergent micelles (i.e., solubilized by sodium cholate), and SMALPs was measured by DSC. For DMPC in different self-assembled SMALP components, SMALP fractions were collected from SEC runs as described earlier. Fraction collection was repeated nine times, and the fractions of the same elution volumes in all runs were combined. The pooled fractions were lyophilized and rehydrated in 0.5 mL of Millipore water. DLS studies confirmed that lyophilization and rehydration do not change the size distributions of the self-assembly nanostructures within individual SMALP fractions. Buffer blanks were prepared by fraction collection, lyophilization, and rehydration in the same manner for use in background subtraction. The DSC measurements were done from 5−70 °C at a heating rate of 2 °C/min using the Nano DSC Microcalorimeter (TA Instrument, New Castle, DE). A total of 6 repeated scans were performed, i.e., 3 cycles of heating and cooling, respectively. Essentially no changes were observed among the 3 heating (i.e., scans 1, 3, and 5) or among the 3 cooling scans (i.e., scans 2, 4, and 6), but the heating versus cooling scans were not an inversion of each other (see, for example, Figure S2, SI). This observation suggests that essentially no structural changes occur during the repeated heating cycles, which would otherwise affect the DSC results. The DSC of the 3rd scan (i.e., the second heating scan) of all samples was reported. The data were analyzed with background subtraction using DSCRun (version 4.3.0; firmware version 1.15a).

TEM. SMALP fractions were collected from SEC runs as described earlier. A droplet of 10 μL of sample from chosen fractions was placed on a 200 mesh formvar/carbon grid and allowed to stay for 1 min. The liquid was then wicked off by the edge of a filter paper, immediately followed by staining with 10 μL of 2% uranyl acetate. After 1 min, the uranyl acetate droplet was also wicked off and the grid was allowed to dry. SMALPs were imaged using a Hitachi H-7650 transmission electron microscope (Hitachi High-Tech in America, Dallas, TX) running the AMT Image Capture Engine V602 (AMT Imaging Direct, Woburn, MA) for data collection.

Other Methods. The DLS measurements were performed at 25 °C on a Zetasizer Nano ZSP using 40-μL disposable microcuvettes. Each sample was measured in triplicate, in which each measurement consisted of a number of scans (typically 10−20). The number of scans in a single measurement was set to be automatic, meaning the Zetasizer program determined the number of scans necessary by analyzing the autocorrelation function and its fit. All reported DLS data passed the data quality check criteria set by the Zetasizer program. The volume-based size distribution, intensity-based size distribution, and the averaged diameters were obtained using Zetasizer software (version 8.02; Malvern Instruments, Westborough, MA). The Fourier transform infrared (FT-IR) spectroscopy was measured on a Bruker Tensor 37 spectrometer running Pus 6.5 for data collection (Bruker Scientific LLC, Billerica, MA).

RESULTS AND DISCUSSION

Synthesis and Characterization of Model SMA Copolymers. In the free radical copolymerization of styrene and maleic anhydride, a growing chain terminated with maleic anhydride propagates to styrene with a high reactivity (r_{MS} ∼ 126.5) but hardly to itself (r_{MM} ∼ 0).[78] On the other hand, a growing chain terminated with styrene propagates either to maleic anhydride or to itself, although the latter occurs with a much lower reactivity (r_{SS} ∼ 0.79).[78] This selectivity dictates that the copolymerization of styrene and maleic anhydride has a strong tendency to form alternating copolymers when the initial monomer feeding ratio S/MA ≤ 1. When the initial monomer feeding ratio S/MA > 1, non-alternating SMAhn random copolymers with an S/MA stoichiometric ratio greater than 1 could be obtained, but a compositional drift toward gradient increase of a styrene unit is bound to happen because the maleic anhydride monomer is depleted at a faster rate than styrene. To achieve a relatively homogeneous S/MA stoichiometric ratio among SMAnh chains, a common practice in the petroleum industry is to run the free radical polymerization in a continually stirring tank reactor maintained at an equilibrium state by feeding a stable ratio of styrene and maleic anhydride monomers. This process produces SMAnh chains with a relatively homogeneous S/MA ratio as long as the corresponding steady-state equilibrium is maintained, but the resultant polymers have poorly controlled chain lengths. The SMA copolymers used in most SMALP studies are derived from commercial SMAnh produced in this manner with high polydispersity indices (typical $Đ$ ∼ 2−3), which contribute to their heterogeneous detergency.

The polydispersity of SMA copolymers can be greatly improved when SMAnh is synthesized via controlled/"living" free radical polymerization methods, such as RAFT polymerization.[25,63,73] The caveat, however, is the inevitable compositional drift as the conversion increases.[63] Iterative RAFT polymerization helps mitigate the drift at the cost of deteriorating $Đ$ as the iteration cycles increase.[66] We chose to mitigate the compositional drift by maintaining a low level of conversion (i.e., ∼20%).[73] Target molecular weight and

https://doi.org/10.1021/acs.biomac.3c00034
Biomacromolecules 2023, 24, 1819−1838

S/MA ratio of SMAnh are reached by carefully optimizing the polymerization conditions, such as the monomer feeding ratio, monomer-to-DATC ratio, concentrations, solvent, and temperature. In this study, we prepared RAFT SMAnh with a similar S/MA ratio (i.e., ∼2/1) but three different chain sizes. For simplicity, we refer to the different RAFT SMAnh as *s*, *m*, and *l* according to their $\overline{M_n}$ estimated from conversion analysis at ∼3, 6, and 12 kDa, respectively, and the RAFT SMA by the same notation of their SMAnh precursors. For example, RAFT SMA-*m* refers to the SMA derived from RAFT SMAhn-*m* that has $\overline{M_n}$ ∼ 6 kDa based on conversion analysis. We used Lipodisq SMAnh that has the same S/MA ∼ 2/1 ratio as control because commercial SMA copolymers with this S/MA ratio are the most frequently used ones in SMALP studies.[59] Besides determining the $\overline{M_n}$ of RAFT SMAnh by conversion analysis, the $\overline{M_n}$, Đ, $\overline{M_v}$, and S/MA were also determined by NMR and SEC analysis (Figure 1a,b; Figure S1, SI). A summary of the structural characteristics of model SMAnh is shown in Table 1.

Table 1. Molecular Weight (in kDa), Polydispersity, and S/MA Ratio of Model SMAnh

SMAnh	$\overline{M_n}^a$	$\overline{M_n}^b$	$\overline{M_n}^c$	Đ^c	$\overline{M_v}^c$	S/MA^b
RAFT SMAnh-*s*	3.0	5.6	20	1.05	36	1.7
RAFT SMAnh-*m*	6.0	7.4	43	1.05	65	1.9
RAFT SMAnh-*l*	12.0	8.4	51	1.06	94	1.9
Lipodisq SMAnh	(2.8[d])		15	2.57		1.9

Determined by [a]conversion, [b]NMR, [c]SEC analysis, respectively. [d]Reported by Malvern Cosmeceutics.

In contrast to Lipodisq SMAnh, which has a large Đ, all RAFT SMAnh show well-defined chain sizes (Đ ∼ 1.05, Table 1). For example, SEC profiles of RAFT SMAnh-*m* and Lipodisq SMAnh are shown (Figure 1b). The Đ of Lipodisq SMAnh was determined to be 2.57 by SEC, which is close to that provided by Malvern Cosmeceutics (i.e., Đ ∼ 2.68). The molecular weight of the same SMAnh determined by different methods differs due to different sources of errors (Table 1). For example, the $\overline{M_n}$ of Lipodisq SMAnh determined by SEC (i.e., 15 kDa) is 5−6 times greater than that reported by Malvern Cosmeceutics (i.e., 2.8 kDa). The same is true for the $\overline{M_n}$ of RAFT SMAnh determined by SEC in comparison to that estimated from conversion or NMR analysis, suggesting that systematic errors exist in the SEC method. Nevertheless, the relative sizes of SMAnh determined by any given method are consistent (Table 1). The S/MA ratio of SMAnh was also determined by NMR (Figure 1; Figure S1, SI), and the NMR method was validated by comparing the measured S/MA ratio of Lipodisq SMAnh (i.e., 1.9) with that reported by Malvern Cosmeceutics (i.e., 2).

The complete hydrolysis of SMAnh to SMA was confirmed by FT-IR spectroscopy, where the peak absorbance of carbonyl stretching was shifted from 1776 to 1711 cm^{-1} when SMAnh was converted to SMA (Figure 1c). For a subset of RAFT SMA, a fluorescent Alexa Fluor 647 tag was successfully conjugated, as shown by fluorescent spectroscopy of SMA-AF647 (Figure 1d).

Heterogeneous Structures in SMALPs. Despite the structural diversity of SMAs or SMA-like copolymers and the target membranes, a fairly simple and straightforward preparation protocol was adopted in most studies of SMALPs or SMALP analogues.[24−28,44−61,63−69] It generally involves mixing stock solutions of copolymer and membrane in a buffer (for example, 20 mg/mL liposomes and 2.5% (wt/vol) of SMA in a phosphate buffer),[59] incubating to allow membrane solubilization, and characterization of membrane solubilization by a series of tools such as DLS, DSC, TEM, and ^{31}P-NMR etc. Although the important effect of amphiphilic balance, such as the S/MA ratio[59−63] and chain size[63−66] on SMALP formation, has been well documented and the polydisperse nature of synthetic polymers is well known, the resultant polymer−lipid nanoparticles are oftentimes simply regarded as LNDs irrespective of the difference in the copolymers being used. To better understand the potential structural heterogeneity, we studied SMALP formation at different P/L weight ratios ranging from ∼12/1 to 1/12, which correspond to P/L molar ratios ranging from ∼1/1 to 1/140 for the SMALPs consisting of RAFT SMA-*m* and DMPC, and characterized the self-assembled polymer−lipid nanoparticles by SEC. An example of the SEC elution profiles of SMALPs comprised of DMPC and RAFT SMA-*m* is shown (Figure 2a). The elution was monitored by both RI and UV-Vis detectors, and column calibration was done using protein standards of known Stokes diameters (shown on the top) run under the same configurations. The Stokes diameter or hydrodynamic diameter (D_h) is defined as the diameter of an equivalent hard sphere diffusing at the same rate as the SMALP component under observation, which can be measured by DLS. Depending on the shape of the SMALPs component, its Stokes radii could be nearly identical to its radius of gyration (R_g, which can be measured by the MALS detector) when the SMALP component is a nanodisc, or ∼1.5 times larger than its R_g when the SMALP component is a homogeneous globular particle.[7] We should be mindful that although SEC separation is a hydrodynamic technique that separates SMALP components based on their Stokes diameters, the elution band at a particular Stokes diameter does not always reflect its size in terms of R_g because of the shape effect. We should also be mindful that while RI is sensitive to capturing the concentration change of all self-assembled structures, caution should be taken on UV-Vis absorbance as it is only sensitive to the concentration change of a particular component that has peak absorbance at the chosen wavelength, hence potentially missing the comprehensive picture of SMALP formation. In addition, the intensity of signals measured by any detector is concentration dependent. Monitoring a 20 μL injection in SEC may artificially miss some elution features of the SMALPs because their absolute concentration is too low to be "visible". Finally, different elution features of the SMALPs may show different sensitivities to a specific detector due to their different compositions, such that some features may appear artificially low (or non-existence) in quantity when compared to other features.

SEC data clearly reveal the heterogeneous nature of SMALPs (Figure 2a). The self-assembled products could be roughly divided into three elution bands, i.e., the L-, M-, and S-band with corresponding hydrodynamic diameters d >17.0 nm, 4.6 < d < 17.0 nm, and d < 4.6 nm, respectively. At low P/L weight ratios (i.e., P/L = 1/3 or lower), only the L- and S-band were observed. The L-band eluted as a single peak (i.e., void volume) irrespective of actual sizes (e.g., d ∼ 33 nm at P/L = 1/3; Figure S3, SI) is tentatively attributed to SMA-remodeled liposomes, i.e., liposomes doped with too few SMA copolymers to reach the point of fragmentation. The S-band is

https://doi.org/10.1021/acs.biomac.3c00034
Biomacromolecules 2023, 24, 1819−1838

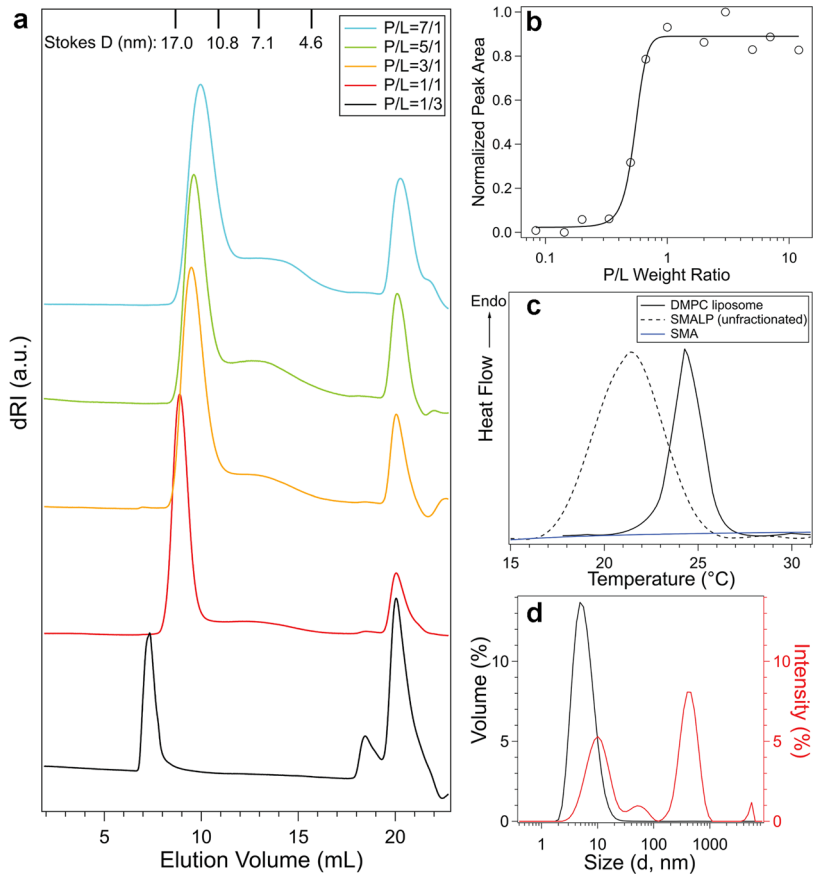

Figure 2. Characterization of SMALPs consisting of RAFT SMA-*m* and DMPC. (a) SEC elution profiles of SMALPs (20 μL injection, prefiltered through a 0.2 μm filter) prepared at different P/L weight ratios as monitored by the RI detector reveal the heterogeneity of SMALPs. The protein markers thyroglobulin, β-amylase, albumin, and carbonic anhydrase with known Stokes diameters at 17.0, 10.8, 7.1, and 4.6 nm, respectively, are shown on the top. (b) The normalized ^{31}P-NMR peak area of as-prepared SMALPs at different P/L weight ratios. (c) DSC of as-prepared SMALPs at a P/L weight ratio of 3/1 (dotted trace in black), DMPC liposome (solid trace in black), and SMA by itself (solid trace in blue). (d) DLS of volume-based (black trace) and intensity-based (red trace) size distribution of the as-prepared SMALPs at a P/L weight ratio of 3/1.

tentatively attributed to SMA-dominant structures, i.e., SMA copolymers that were eluted predominantly by themselves. The neatly separated elution of liposome-dominant and polymer-dominant structures at low P/L weight ratios suggests a very low level of liposome solubilization by the SMA copolymers at those ratios. This attribution is supported by the observation that as the P/L weight ratio increases, the S-band remains essentially unchanged in position, while the L-band disappears and nanostructures of different sizes appear in the M-band, suggesting the morphological change of liposomes beyond a critical P/L weight ratio to form polymer−lipid nanoparticles of different sizes. Despite the fact that more SMA copolymers are involved in solubilizing liposomes at higher P/L weight ratios, we still observe a seemingly increasing magnitude of the S-band as the P/L weight ratios increase from 1/1 to 7/1, which may simply reflect the fact that increased amount of SMA copolymers is present in the system. It should be noted that a quantitative comparison of the absolute magnitude of any elution band across different SMALP samples is not appropriate because they were prepared at different P/L weight ratios. A more reasonable approach would be to compare the magnitude of a SMALP elution band to the band of an internal calibration standard that is kept the same across different samples, but we do not have any elution band that can serve this purpose. To complicate the matter more, larger, undissolved liposomal structures in SMALPs prepared at very low P/L weight ratios could be filtered out before entering the SEC column to even show up in the chromatogram, such that the S-band in those SMALPs appears artificially high in comparison to their L-band, as shown for the P/L = 1/3 sample (Figure 2a).

The existence of a critical P/L weight ratio beyond which maximum solubilization of liposomes occurs agrees with previous observations.[60] This ratio was determined by ^{31}P-NMR spectroscopy to be ∼1/1 for RAFT SMA-*m* (Figure 2b) because the increase of ^{31}P peak areas of the as-prepared SMALPs (i.e., unfractionated SMALP products) that reflects the generation of small, fast-tumbling polymer−lipid nanoparticle plateaus out beyond this P/L weight ratio. In the plateau regime (e.g., at *a* P/L weight ratio of 3/1), decreased DMPC gel-to-liquid crystalline transition temperature from a sharp peak centered at ∼24.5 °C for intact liposomes to a broad one centered at ∼21.5 °C for as-prepared SMALPs was observed by DSC (Figure 2c), indicating disrupted packing of DMPC by SMA copolymers. Note that SMA copolymer by itself does not show any phase transition in this temperature range (Figure 2c). The formation of polymer−lipid nanoparticles is further confirmed by DLS, where the volume-based size distribution of as-prepared SMALPs reveals a single peak centered at ∼5 nm (Figure 2d), in contrast to intact DMPC liposomes showing a peak size centered at ∼140 nm (Figure S3, SI). The single DLS peak in the volume-based size

https://doi.org/10.1021/acs.biomac.3c00034
Biomacromolecules 2023, 24, 1819−1838

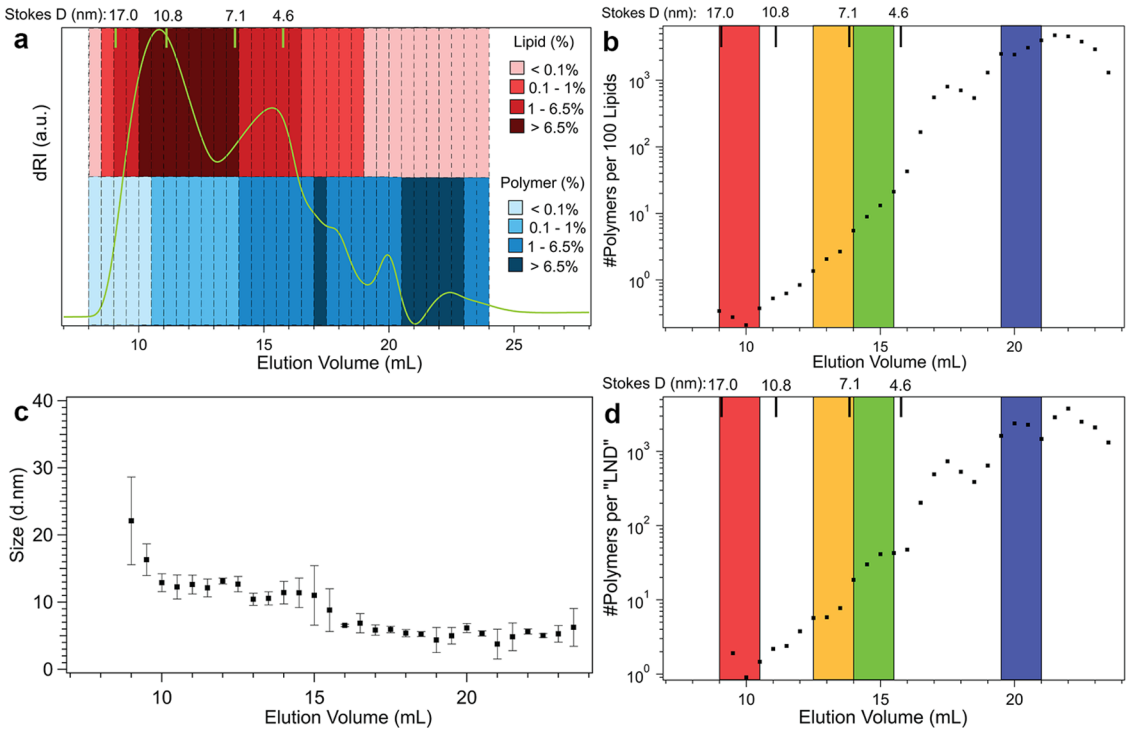

Figure 3. P/L stoichiometric ratios in SEC fractions of SMALPs greatly help illuminate their heterogeneous structures. (a) The SEC elution profile (green trace) of SMALPs (500 μL injection, prefiltered through a 0.2 μm filter) consisting of RAFT SMA-*m* and DMPC prepared at a P/L weight ratio of 3/1 as monitored by the RI detector. Protein markers that run under the same conditions are shown on the top. The elution volumes were collected into a series of 0.5 mL of fractions as delineated by the dotted lines, and the same fractions from multiple SEC runs were combined to collect sufficient samples as explained in Methods. Within each fraction, the percentage mass of DMPC (red) and SMA (blue) with reference to their respective total mass in all recovered fractions were determined and are shown in shaded color bars denoting the different percentage ranges as listed on the right. (b) The number of polymer chains (n_{poly}) per 100 lipids in individual SMALP fractions increases steadily as the elution volume increases (i.e., SMALP sizes decrease), indicating the coexistence of a wide range of self-assembled polymer−lipid nanostructures. Representative 1.5 mL fractions at 9−10.5, 12.5−14, 14−15.5, and 19.5−21 mL showing n_{poly} per 100 lipids smaller than 1, 1−10, and 10−100, and greater than 1000, respectively, are marked by red, yellow, green, and blue zones. (c) The average diameters of individual 0.5 mL fractions of SMALPs measured by DLS. (d) Assuming the self-assembled nanostructures in each SMALP fraction are pseudo LNDs, the number of SMA chains per "LND" is computed. The same 1.5 mL fractions marked by red, yellow, green, and blue zones show n_{poly} per "LND" close to 1, 10, 100, and 1000 or more, respectively. Obviously, not all of the n_{poly} per "LND" numbers can fit the LND model. We attribute the major components in each fraction to polymer-remodeled liposomes, polymer-encased LNDs, polymer−lipid mixed micelles, and lipid-doped polymer micellar aggregates, respectively. Note: Individual 0.5 mL fractions in (b−d) are represented at the start of their elution volumes, e.g., fraction 9−9.5 mL is represented at 9 mL.

distribution of SMALPs (Figure 2d) may create an illusion that the SMALPs are "homogeneous" or even "monodisperse". This illusion could get carried away further as both ^{31}P-NMR (Figure 2b) and DSC (Figure 2c) are not able to tell the size variations among polymer−lipid nanoparticles in the as-prepared SMALPs. Nevertheless, the heterogeneity of SMALPs is in clear display in SEC (Figure 2a) and intensity-based size distribution of DLS (Figure 2d).

It should be noted that the heterogeneity of SMALPs at a given P/L weight ratio, as revealed by SEC, reflects the true nature of SMALPs, not some temporary artifacts caused by the dilution-induced structural changes during the SEC procedure. The SEC traces of SMALPs prepared at different P/L weight ratios that were diluted during the SEC runs (Figure 2a) are in complete agreement with the ^{31}P-NMR study of their as-prepared SMALPs that were not diluted (Figure 2b). For example, the ^{31}P-NMR study of the as-prepared SMALPs at P/L = 1/3 shows the negligible contribution from nanostructured SMALPs (Figure 2b). This aspect is faithfully reflected in the SEC elution profile of the same SMALPs (Figure 2a, black trace), where only SMA-remodeled liposomes (i.e., L-band) and SMA-predominant elution (i.e., S-band) are observed but not the nanostructured SMALPs (i.e., M-band), indicating that the SMA-remodeled liposomes did not become nanostructured SMALPs due to dilution during the SEC run. The absence of SEC-dilution-induced structural change of this sample is also evident in the DLS study (Figure S3b, SI), where the DLS of as-prepared SMALPs shows the presence of large SMALP structure consistent with its SEC elution profile (Figure 2a). Additionally, for SMALPs beyond the critical P/L weight ratio (i.e., 1/1, 3/1, 5/1, and 7/1), the ^{31}P-NMR study of the as-prepared SMALPs shows the presence of a plateaued level of nanostructured SMALPs (Figure 2b), which is also consistent with their SEC traces that reveal a stable presence of the M-band (Figure 2a), suggesting the nanostructured SMALPs (i.e., M-band) do not undergo significant structural changes to become S-band or L-band due to dilution during the SEC runs.

Interestingly, the polymer−lipid nanoparticles in the M-band are collectively and continuously downsized at increasing P/L weight ratios, as witnessed by the continuous shift of their distribution toward a smaller size range (Figure 2a; Figure S3, SI), underscoring a dynamic equilibrium among the different polymer−lipid self-assembled structures toward more solubi-

https://doi.org/10.1021/acs.biomac.3c00034
Biomacromolecules 2023, 24, 1819−1838

lized states as the P/L weight ratios increase. Similar SEC features that show the heterogeneity of SMALPs and the continuous downsizing of polymer−lipid nanoparticles at increasing P/L weight ratios were observed for all SMA copolymers, including the Lipodisq SMA (Figure S4, SI). This downsizing behavior was also reported in previous studies of SMALPs[60,66,79] and SMALP analogues,[27,28,53] in which "macro-nanodiscs" were sometimes used to refer to the self-assembly products obtained at low P/L weight ratios that show peak diameters greater than ∼20 nm in DLS.[28,53] As we discussed earlier, speculation of SMALP structures based on size data revealed in DLS has its limit when heterogeneous structures exist. To gain a better understanding of SMALPs, it is imperative to separate the different self-assembled components first before meaningful evaluation can be made to assess whether they truly resemble the bilayer structure of nanodiscs.

***P/L* Stoichiometric Ratios of Fractionated SMALPs Shed Light on Their Different Structures.** We used SEC to fractionate the SMALPs comprised of RAFT SMA-*m* and DMPC prepared at a P/L weight ratio of 3/1. The polymer and membrane were fluorescently labeled with AF647 and NBD-PE, respectively, and the concentrations of SMA and DMPC in individual SMALP fractions were determined by fluorescent spectroscopy based on calibration curves built on the fluorescently tagged SMA copolymer and DMPC membrane themselves (Figure S5, SI). To account for the potential fluorescent bleaching during sample preparation and characterization, we obtained the percentage mass of SMA and DMPC, respectively, in individual SMALP fractions with reference to their total mass in all recovered fractions as determined by the fluorescent spectroscopy (Figure 3a). The fraction collection was stopped at the column bed volume (i.e., V_e = 24 mL). Any residue lipid and polymer eluted after this volume is expected to be negligible. Assuming 100% recovery of the starting materials, the recalibrated mass of SMA and DMPC in each fraction were obtained, and the P/L stoichiometric ratios in individual SMALP fractions were computed based on the molecular weight of SMA-*m* and DMPC, respectively (Figure 3b). Given that the $\overline{M_n}$ of synthetic polymers determined by different methods differ, we chose to use the $\overline{M_n}$ of SMA-*m* (∼7.8 kDa) derived from its RAFT SMAnh-*m* precursor determined by NMR (i.e., ∼7.4 kDa) because it is close to what is expected from the conversion analysis (Table 1). Just like the reported $\overline{M_n}$ of Lipodisq SMAnh, this $\overline{M_n}$ is 5−6 times smaller than that determined by SEC (Table 1) due to the systematic error in the SEC method. We further determined the average diameters of the polymer−lipid nanoparticles in individual SMALP fractions by DLS (Figure 3c). Assuming that the self-assembled nanoparticles in all SMALP fractions are pseudo LNDs (which are unlikely true, by the way), we calculated the number of polymer chains involved in forming individual "LNDs" (Figure 3d) of different sizes based on their respective P/L stoichiometric ratios and a simple geometric model, in which the diameters of "LNDs" were related to the number of lipids fit within each leaflet of "LNDs" by dividing the surface areas of individual "LNDs" with the headgroup area of DMPC (i.e., ∼0.606 nm^2).[80] This quantitative analysis of P/L stoichiometric ratios in individual SMALP fractions greatly helped illuminate their different polymer−lipid self-assembled nanostructures.

The first and foremost discovery from quantifying the polymer and lipid in fractionated SMALPs is that they are distributed unevenly within a range of polymer−lipid nanostructures of different sizes (Figure 3a). Most DMPC rests in fractions within 8.5−19 mL, whereas most SMA rests in fractions within 10.5−24 mL. The beginning and end of the elution volume at V_e < 10.5 mL and V_e > 19 mL, respectively, are populated predominantly by DMPC and SMA, echoing our earlier assessment that lipid represents the primary component in the L-band of SMALP elution, whereas a polymer represents the primary component in the S-band. Among all of the 0.5 mL fractions that show the presence of lipids, DMPC is concentrated in 9−16.5 mL fractions (i.e., >1% per fraction) and heavily concentrated in 10−14 mL fractions (i.e., >6.5% per fraction). Among all of the 0.5 mL fractions that show the presence of a polymer, SMA is concentrated in 14−24 mL fractions (i.e., >1% per fraction) and heavily concentrated in 20.5−23 mL fractions (i.e., >6.5% per fraction). This misaligned abundance distribution of DMPC and SMA in SMALP components of different sizes suggests that not all polymer−lipid nanostructures are co-assembled in the same manner. More structural insight into the different SMALP components would benefit from quantitative analysis of the P/L stoichiometric ratios in individual SMALP fractions.

Given that LNDs with a diameter of ∼10 ± 1 nm would hold ∼250 ± 100 lipids depending on the headgroup areas of lipids,[6,7] the P/L stoichiometric ratios within individual 0.5 mL fractions of SMALPs are presented as the number of SMA chains (n_{poly}) associated with every 100 DMPC lipids (Figure 3b). Clearly, not all SMALP components are created the same. There is an almost linear increase of n_{poly} per 100 lipids (in log-scale) in the M-band of SMALP elution as the polymer−lipid nanoparticles decrease in sizes from 17.0 to 4.6 nm, indicating the coexistence of a wide range and increasingly solubilized membrane structures characterized by more and more thorough intermixing between the SMA and DMPC. This linear increase of n_{poly} per 100 lipids (in log-scale) takes a steep upward turn and plateaus in the S-band of the SMALP elution when the nanoparticle sizes drop below 4.6 nm, again reaffirming our earlier assessment that the S-band consists primarily of the SMA copolymer by itself. The different SMALP structures could be roughly divided into four regions characterized by their significantly different n_{poly} per 100 lipids, i.e., n_{poly} < 1, 1 < n_{poly} < 10, 10 < n_{poly} < 100, and n_{poly} > 100, respectively, that underlie their potentially very different structures. Representative 1.5 mL fractions in each region marked by red, yellow, green, and blue zones (Figure 3b) are selected for further structural characterization.

To gain additional structural insight into SMALPs, we measured the average diameters of SMALPs in individual 0.5 mL fractions (Figure 3c). Assuming that the SMALPs in each fraction are equivalent to a pseudo LND with the same average diameter of that fraction, we computed n_{poly} per "LND" (Figure 3d) as an intuitive aid to help comprehend whether the LND hypothesis would hold for each SMALP fraction. The same 1.5 mL fractions marked by red, yellow, green, and blue zones, respectively, still represent nicely the potentially very different structures that show ∼1 order of magnitude increase in n_{poly} per "LND" from one zone to the next. In the red zone at the beginning of the M-band, where the SMALPs show an average diameter of d ∼ 17 ± 5 nm, the n_{poly} per "LND" hovers around 1. Considering that the $\overline{M_n}$ of RAFT SMA-*m* only allows a maximum chain length (i.e.,

https://doi.org/10.1021/acs.biomac.3c00034
Biomacromolecules 2023, 24, 1819−1838

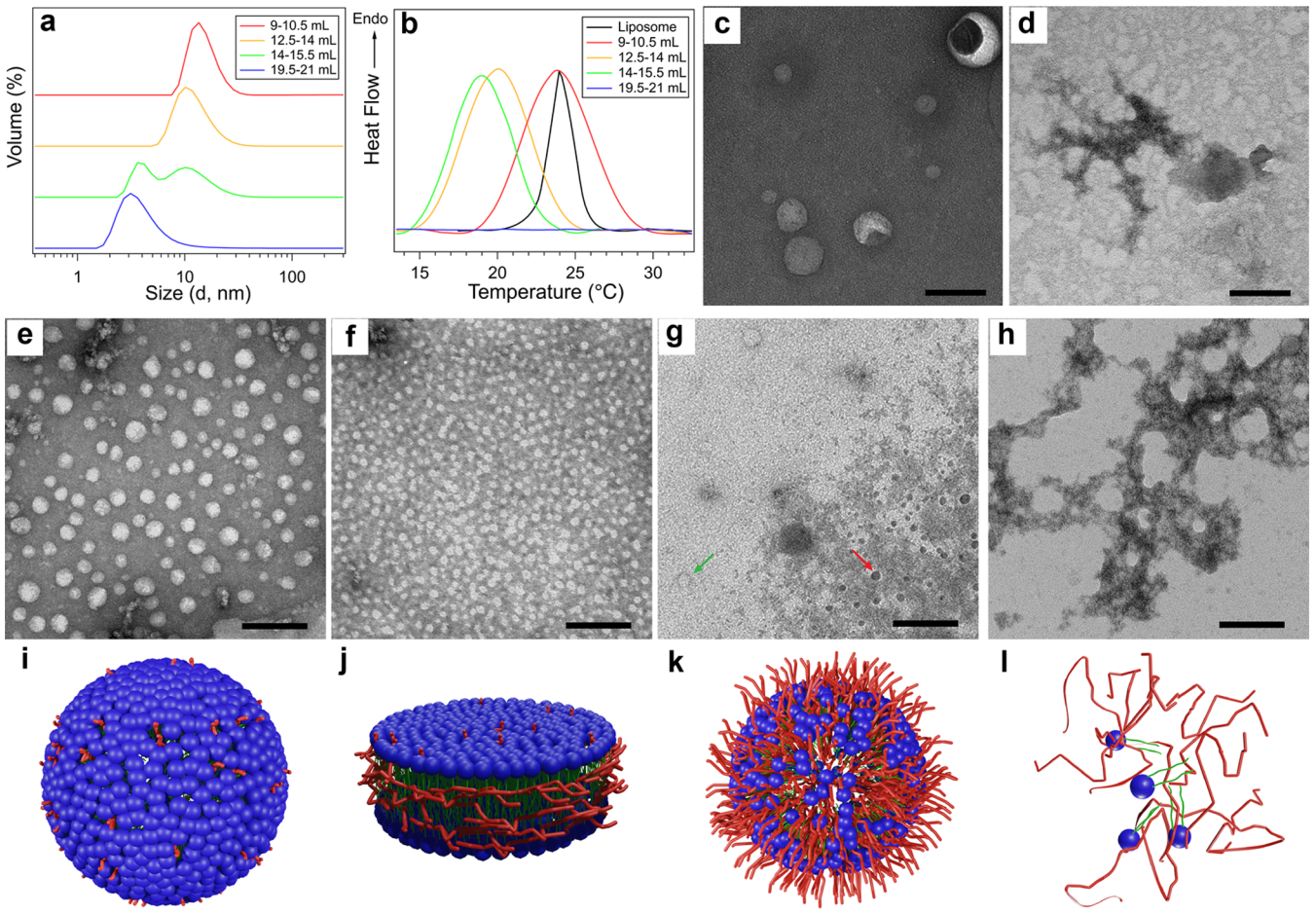

Figure 4. Characterization and determination of the heterogeneous structures in SMALPs. Representative 1.5 mL fractions marked by red, yellow, green, and blue zones in the SEC elution of SMALPs prepared at a *P*/*L* weight ratio of 3/1 (Figure 3) were collected and characterized by (a) DLS, (b) DSC, and (e−h) TEM, respectively, while the TEM of the intact DMPC liposome (c) and RAFT SMA-*m* (d) by itself are also shown as controls (scale bar in c−h: 100 nm). The four representative SMALP structures that exist predominantly in the four colored zones are confirmed and schematically illustrated: (i) polymer-remodeled liposomes, (j) polymer-encased LNDs, (k) polymer−lipid mixed micelles, and (l) lipid-doped polymer micellar aggregates. The lipid headgroup and tail are shown in blue and green, respectively, and polymer chains are shown in red.

contour length) estimated to be ∼17 nm, it would be physically impossible for 1 SMA chain to encase any "LND" in this zone, suggesting that SMALPs in the red zone are not nanodiscs after all. Considering a very small *P*/*L* stoichiometric ratio of ∼0.002 in this zone (Figure 3b), we tentatively assign SMALPs in this zone to SMA-remodeled liposomes, i.e., transformed liposomes in polymer-doped states with significantly reduced sizes, possibly caused by the change of surface tension due to membrane disruption by SMA. We do not believe that the SMA-remodeled liposomes are "macro-nanodiscs" because the n_{poly} per "LND" is simply too small to support the nanodisc model. These polymer-doped and disrupted liposome structures may well be anisotropic, which would allow magnetic alignment for structural studies by NMR.[28]

As the elution volume increases and the polymer−lipid nanoparticles decrease in size, the n_{poly} per "LND" continuously increases and reaches two small intermediate plateaus in the M-band of SMALPs that are leveled close to ∼10 and ∼100, respectively, before taking a steep upward turn and reaches its final plateau in the S-band of SMALP elution (Figure 3d). In the first small plateau that coincides with the yellow zone, the averaged diameters of SMALPs are ∼10 ± 1 nm as measured by DLS (Figure 3c), and the n_{poly} per "LND" is close to 10. This number does support the presence of polymer-encase LNDs because if we consider that each LND in MSP-encased LNDs is stabilized by 2 MSP chains[6,7] and the chain length of MSP (e.g., MSP1 has 212 amino acid residues) is at least twice that of SMA-*m* (e.g., SMA-*m* has 69 repeating units), we would expect to have at least 4 SMA-*m* chains to stabilize each LND, plus possibly additional SMA chains that are doped into the lipid membrane but do not yet reach the point of membrane partition as shown by the SAXS analysis.[68] Interestingly, if we assume the SMALPs eluted between ∼12−14 mL to consist primarily of polymer-encased LNDs, ∼41.3 wt % of lipids and ∼3.2 wt % of SMA copolymers, respectively, of this particular SMALP preparation (i.e., *P*/*L* weight ratio = 3/1) are found to be involved in the formation of polymer-encased LNDs (Figure 3a), suggesting that the majority of SMA copolymers needed to solubilize the membranes do not contribute to the formation of LNDs. In the second small plateau that coincides with the green zone, the average diameter of SMALPs is ∼7 ± 3 nm (Figure 3c), and the n_{poly} per "LND" approaches ∼100. Although not entirely impossible, we believe nanodisc is no longer an appropriate structural model to represent most SMALPs in this zone. Instead, they could be best described as

https://doi.org/10.1021/acs.biomac.3c00034
Biomacromolecules 2023, 24, 1819−1838

polymer−lipid mixed micelles based on their closely matched P/L stoichiometric ratios (i.e., 0.1−1, Figure 3b).

As the elution volume increases further, the average diameters of SMALPs are reduced to ∼3 ± 1 nm (Figure 3c), and the n_{poly} per "LND" increases steeply to plateau at the order of ∼1000 in the S-band of SMALP elution, as highlighted by the blue zone (Figure 3d). It is physically impossible to encase such small "LNDs" with 1000 or more SMA chains, suggesting that "LNDs" unlikely exist in the S-band. The presence of lipids, albeit significantly outnumbered by the polymer (P/L > 10, Figure 3b), can still be undeniably confirmed (Figure 3a). We believe that SMALPs in the S-band are lipid-doped polymer micellar aggregates consisting predominantly of SMA chains that manage to rip some lipids off the membrane but fail to fully participate in membrane solubilization, possibly due to undesirable detergency, limited self-assembly kinetics, and/or a surplus of the polymer.

To test the structural insight inferred from quantitatively determined P/L stoichiometric ratios in individual SMALP fractions of different sizes, we collected the representative SMALP elution fractions as marked by red, yellow, green, and blue zones, respectively, as discussed earlier (Figure 3), and examined them using a series of complementary characterization tools such as DLS, DSC, and TEM (Figure 4). Although none of these tools can tell unambiguously any specific structure in SMALPs, together they provide consistent evidence that corroborates the presence of the four very different characteristic SMALP structures as inferred from the analysis of their respective P/L stoichiometric ratios.

In DLS (Figure 4a) and DSC (Figure 4b), the same quadruple color scheme was used to represent the pooled 1.5 mL fractions selected from the four different elution zones as shown in Figure 3b. DLS of the pooled 1.5 mL fractions from the SMALP elution still shows nicely the continuous decrease of polymer−lipid nanoparticle sizes as elution volume increases (Figure 4a), reaffirming that the self-assembled structures in the four selected elution zones differ from each other. Notably, for the green zone fraction where an expected transition from polymer-encased LNDs in the adjacent yellow zone (i.e., n_{poly} per "LND" ∼10; Figure 3d) to polymer−lipid mixed micelles (i.e., n_{poly} per "LND" ∼100) occurs, a bimodal size distribution of SMALPs was observed, suggesting the coexistence of different populations of polymer−lipid self-assembled nanostructures in this zone.

DSC of the four representative 1.5 mL fractions as compared to intact DMPC liposomes (shown in black) sheds new light on the structures of the different SMALP components (Figure 4b). For the red zone at the beginning of the M-band of SMALPs, the same transition temperature as that of intact liposomes at ∼24.5 °C is revealed (red trace), but the peak width is much broader, corroborating our earlier assessment that SMALPs in this zone are SMA-remodeled liposomes that have not reached the point of membrane fragmentation yet, as the unchanged transition temperature indicates unfragmented membrane, while the broadened peak indicates perturbated lipid−lipid interactions due to polymer insertion. DSC of the blue zone fraction from the S-band of SMALP elution does not show any trace of lipid phase transition (blue trace), again corroborating our earlier assessment that SMALPs in this zone are lipid-doped polymer micellar aggregates that do not contain sufficient lipid−lipid interactions to reveal a transition temperature. DSC of the yellow and green zones in the M-band of SMALP elution that presumably constitute mainly of polymer-encased LNDs and polymer−lipid mixed micelles (yellow and green traces), respectively, do show reduced transition temperatures centered at ∼20 and ∼18.8 °C together with broadened peaks, indicating membrane solubilization and disrupted lipid−lipid packings. The further reduced transition temperature of SMALPs in the green zone as compared to that in the yellow zone supports our earlier assessment that SMALPs in the green zone consist of more solubilized forms of the membrane (i.e., increased polymer−lipid intermixing). The broadened phase transition peak and reduced phase transition temperature of lipids in SMALPs or SMALP analogues as compared to that in intact liposomes have been frequently reported.[27,69] It should be pointed out that this change of lipid phase transition behavior by itself only reflects membrane solubilization and disrupted lipid−lipid packing; it does not necessarily support the formation of LNDs. As a matter of fact, broadened phase transition peaks and continuously reduced transition temperatures of DMPC are also observed when it is solubilized by increasing concentrations of sodium cholate to form DMPC-cholate mixed micelles (Figure S6, SI). The reduced phase transition temperature of lipids in SMALPs or SMALP analogues underscores the disruptive nature of polymer solubilization to the target membrane akin to detergent solubilization, which is likely caused by the relatively high detergency of SMA or SMA-like copolymers. In contrast, the phase transition temperature of lipids in MSP-encased LNDs is increased as compared to that in intact liposomes,[81] suggesting restricted thermal motion of lipids, likely caused by the confinement effect of MSPs when they have less detergency than SMA or SMA-like copolymers to instigate membrane disruptions.

The different self-assembled nanostructures distributed among the four representative 1.5 mL fractions in the SEC elution of SMALPs (Figure 3b) are further confirmed by TEM. TEM of intact DMPC liposomes and SMA polymers before their co-assembly are also shown as controls. The small unilamellar vesicles of DMPC appear as spherical gray objects of different sizes ranging from ∼20 to 100 nm (Figure 4c). The gray appearance of the vesicles on the dark background is due to the negative staining by uranyl acetate and the fact that zwitterionic DMPC does not bind uranium ions. Their vesicle form is only serendipitously revealed by the broken ones, as the one shown in the upper right corner in Figure 4c. The SMA copolymer by itself appears as dark patches stretching randomly in different directions under TEM (Figure 4d), with its dark appearance likely caused by the preferential binding of uranium ions to the maleic acid moieties on the copolymer.

The SMALPs at the beginning of the M-band (red zone) appear as spherical gray objects with diameters d ∼ 25 ± 9 nm under TEM (Figure 4e), most of which have significantly reduced sizes from their liposome precursors. As we discussed earlier, these SMALPs are attributed to polymer-remodeled liposomes schematically illustrated (Figure 4i) beneath the TEM micrograph because their P/L stoichiometric ratios are too low to possibly encase the lipids as "macro-nanodiscs" (Figure 3b,d), and DSC also confirmed that they have the same phase transition temperature as that of intact liposomes (red trace, Figure 4b). Moving forward into the middle of the M-band (yellow zone), the SMALPs appear as spherical gray objects with nearly homogeneous diameters d ∼ 10 ± 2 nm (Figure 4f), which match well our earlier assessment that they consist mainly of polymer-encased LNDs, as schematically illustrated beneath (Figure 4j). As the elution volume increases

https://doi.org/10.1021/acs.biomac.3c00034
Biomacromolecules 2023, 24, 1819−1838

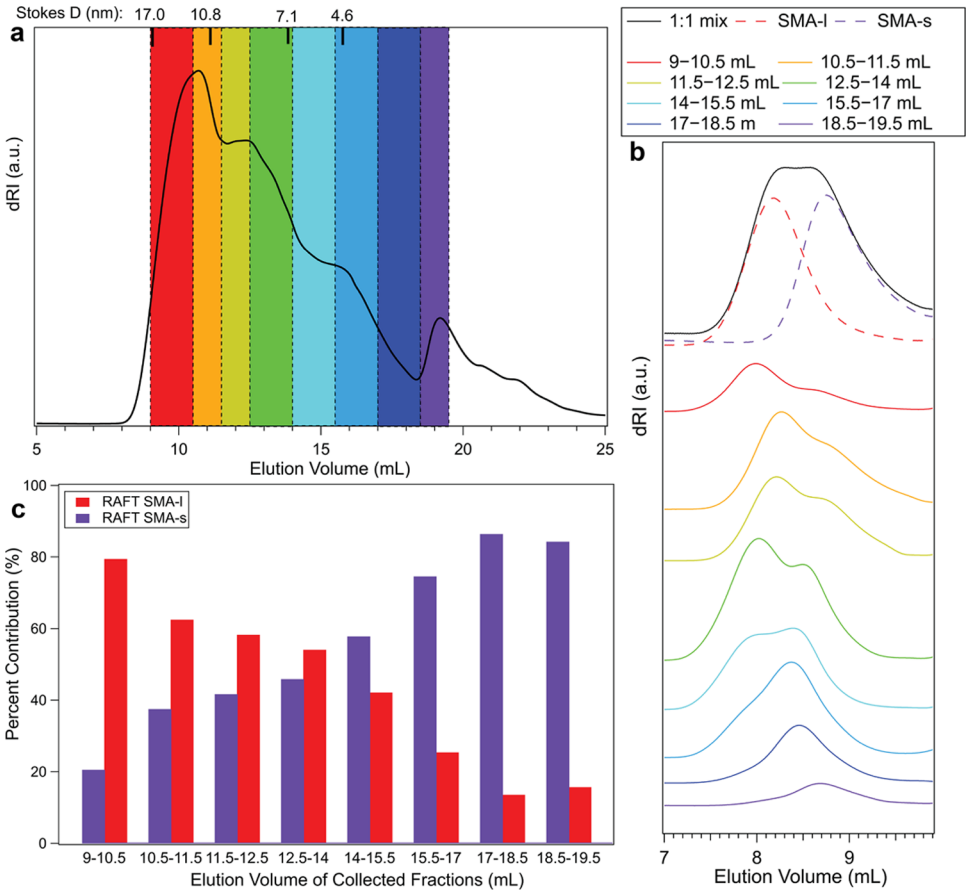

Figure 5. SMA copolymers with a similar *S*/MA ratio but different chain sizes show their preferential contribution to the formation of different SMALP structures. (a) SEC elution profiles of SMALPs (500 μL injection, prefiltered through a 0.2 μm filter) consisting of DMPC and a 1:1 (weight ratio) mixture of RAFT SMA-*l* and SMA-*s*. The SMALPs were prepared at a *P*/*L* weight ratio of 3/1 and monitored by the RI detector (black trace). Protein markers with known Stokes diameter were also run under the same SEC configurations and shown on the top. The elution volumes were collected into a series of fractions with different hydrodynamic diameters as delineated by the dotted lines and denoted in different colors. (b) SEC rerun (20 μL injection, prefiltered through a 0.2 μm filter) of each SMALP fraction in DMF reveals the elution peak of the mixed copolymers. The rerun traces are denoted in the same color scheme as their corresponding SMALP fractions, as shown on the top of this panel and in panel a. As controls, the elution peaks of SMA-*l* (dotted trace in red), SMA-*s* (dotted trace in purple), and their 1:1 mixture (solid trace in black) run in DMF are also shown at the top of this plot. (c) By fitting the elution peaks of mixed copolymers in all SMALP fractions with the respective elution peak of SMA-*l* and SMA-*s* by itself, quantitative contributions (wt %) of SMA-*l* (red) and SMA-*s* (purple) to the formation of different SMALP structures eluted at different volumes are obtained.

further into the end of the M-band (green zone), the majority of SMALPs appear as dark spherical objects with diameters $d \sim 7 \pm 3$ nm (marked by a red arrow, Figure 4g). The unusual dark appearance of these objects reveals their preferential binding to uranium ions, which is only possible with the presence of high-concentration SMA polymers on their surface. This observation is consistent with our earlier assessment that the SMALPs in the green zone consist mainly of polymer−lipid mixed micelles, as schematically illustrated beneath (Figure 4k). Because this zone is bordered by the yellow zone of SMALP elution populated by the polymer-encased LNDs, LNDs did show up as a minor component (marked by a green arrow, Figure 4g), which explains the observed bimodal size distribution in DLS (green trace, Figure 4a). Finally, TEM of the blue zone resting in the S-band of the SMALP elution reveals randomly distributed dark patches (Figure 4h) similar to that of SMA by itself (Figure 4d), agreeing well with our earlier assessment that SMALPs in the blue zone consist mainly of lipid-doped polymer micellar aggregates, as schematically illustrated beneath (Figure 4l).

Mechanistic Insight into the Structural Heterogeneity of SMALPs. We believe the fundamental reason for the observed wide variety of SMALP structures is that not all synthetic polymer chains are created the same. Microstructure variations among individual polymer chains in size, sequence, and hydrophobic/hydrophilic ratio can be constricted using innovative polymerization strategies, but by and large, those variations still exist. As a result, heterogeneous amphiphilic balance among synthetic polymer chains is inevitable, which leads to their polydisperse detergency and dissimilar membrane remodeling behaviors. Since most studies in SMALPs and SMALP analogues use synthetic copolymers that have broad size distributions, we test here the role of chain size in SMALP formation using well-defined SMAs prepared via RAFT polymerization that have a similar *S*/MA ratio but two very different $\overline{M_n}$, i.e., RAFT SMA-*l* and SMA-*s* (Figure S1, SI). Although exception exists,[27] most studies observed that SMA or SMA-like copolymers with smaller $\overline{M_n}$ are more effective in solubilizing membranes into SMALPs[63,64] or nanodiscs.[65,66] Given that the formation of SMALPs also

https://doi.org/10.1021/acs.biomac.3c00034
Biomacromolecules 2023, 24, 1819−1838

depends on the P/L weight ratios under otherwise similar conditions (Figure 2; Figure S4, SI), and that SMALPs are not simply nanodiscs—they rather consist of diverse polymer−lipid self-assembled states that differ in structures (Figures 3 and 4), we decided to solubilize DMPC liposomes using a 1:1 (weight ratio) mixture of SMA-*l* and SMA-*s* at a P/L weight ratio of 3/1, and quantify the contribution from each SMA copolymer to the formation of different SMALP structures (Figure 5). Toward that end, we collected SMALP fractions of different sizes eluted at different volumes, freeze-dried individual fractions, redissolved the residues of each fraction in DMF to separate the SMA copolymers from lipids, re-ran the SEC of each fraction in DMF to obtain the elution peaks of the mixed copolymers, and fit the mixed copolymer elution peaks in all fractions as monitored by the concentration detector (i.e., the RI detector) with the elution peak of SMA-*l* and SMA-*s* by itself.

The SEC elution profile of SMALPs comprised of DMPC and a 1:1 (weight ratio) mixture of RAFT SMA-*l* and SMA-*s* prepared at a P/L weight ratio of 3/1 and monitored by the RI detector is shown in Figure 5a. Again, the self-assembled SMALP structures can be roughly divided into three elution bands, i.e., the L-, M-, and S-band, respectively, based on their hydrodynamic diameters. Since the L-band has a negligible concentration of copolymers (Figure 3a), we collected a series of SMALP fractions with different sizes eluted in the M- and S-band as delineated by the dotted lines and denoted in different colors (Figure 5a). SEC reruns of all collected fractions lyophilized and redissolved in DMF (with 0.01% (v/w) LiBr) as compared to that of SMA-*l*, SMA-*s*, and their 1:1 mixture, respectively, run under the same SEC configurations reveal the mixed SMA copolymer peaks in all collected fractions (Figure 5b), in which a gradual shift from predominant SMA-*l* to predominant SMA-*s* contribution in individual SMALP fractions collected at increasing SMALP elution volumes (i.e., decreasing SMALP sizes) is in clear display.

To quantitatively determine the contribution from SMA-*l* and SMA-*s* to each SMALP fraction, the mixed copolymer peaks in all SMALP fractions were fit with the respective elution peak of SMA-*l* and SMA-*s* by themselves (Figure S7, SI). The concentration detector (i.e., the RI detector) allows quantitative deconvolution of the elution peaks to reveal contributions from each SMA copolymer, and the utility of this method was verified by fitting the elution peak of the 1:1 mixture of SMA copolymers, in which an expected ∼50% contribution from each copolymer was indeed obtained (Figure S7, SI). The percentage weight contribution (i.e., wt %) from each SMA copolymer to the different SMALP fractions is shown (Figure 5c). Although SMA-*l* and SMA-*s* have a similar S/MA ratio and were used in equal weight initially to solubilize liposome membrane into SMALPs, the two copolymers ended up contributing very differently (in wt %) to the formation of the different SMALP structures, underscoring the important effect of the overall amphiphilic balance of copolymer chains on directing specific SMALP formation. SMA-*l* is predominant at the beginning of the M-band (i.e., SMA-remodeled liposomes), whereas SMA-*s* is predominant at the end of the M-band (i.e., polymer−lipid mixed micelles) as well as the S-band (i.e., lipid-doped polymer micellar aggregates). The decreasing SMA-*l* and increasing SMA-*s* contributions to SMALP fractions eluted at higher volumes (i.e., decreasing hydrodynamic diameters toward more polymer-solubilized forms) suggest the increased solubilization power and detergency of smaller SMA under otherwise similar conditions, which agrees with previous observations.[63,64] However, caution should be taken on whether smaller SMA is more effective in solubilizing membranes into nanodiscs as previously suggested.[65,66] Suppose the sizes of SMA-encased LNDs are independent of the SMA chain sizes as reported,[60,62,66] we would expect the LND fractions to appear in the middle of the M-band with Stokes diameters between 10.8 and 7.1 nm as shown earlier (Figures 3 and 4), with corresponding elution volumes between ∼11.5 and 14 mL (Figure 5a). Interestingly, our quantitative analysis shows that SMA-*l* rather than SMA-*s* has a higher wt % contribution to those fractions (Figure 5c). This model study suggests that under otherwise similar conditions, SMA or SMA-like copolymers with more focused size distributions and amphiphilic balances will help reduce the structural heterogeneity of SMALPs or SMALP analogues, as chain size is one important factor that helps define the overall amphiphilic balances of the copolymer chains. As further evidence of this important concept, SMALPs comprised of DMPC and Lipodisq SMA that has a large $Đ$ do show pronounced structural heterogeneity as manifested by the very broad SMALPs elution peaks in the M- and S-band (Figure S4, SI).

Proteorhodopsin Extracted into Different SMALP Structures Shows Different Photocycle Kinetics. One of the most important challenges in membrane biology is to understand the structure and function of membrane proteins in their native states. Since different membrane proteins co-exist in cell membranes, oftentimes, an indispensable operation is to extract specific membrane protein from its native membrane by detergent first, followed by reconstitution of the detergent-solubilized protein back into artificial membranes if needed. Detergent solubilization is a rather disruptive process, and concerns always exist on whether the physiologically relevant structure and function of membrane proteins would differ from those solubilized in detergent micelles or reconstituted in artificial membranes.[82−84] Because SMA or SMA-like copolymers can bypass detergent solubilization and extract membrane protein directly from their native membranes, SMALPs or SMALP analogues are hailed as native membrane platforms with great potential in membrane biology.[85,86] This enthusiasm is somewhat dampened by recent studies that questioned the native nanodisc notion by lipidomic[67] and SAXS analysis.[68] Our own data (Figures 2−4; Figure S4, SI) further uncovered the structural heterogeneity and altered lipid−lipid interactions in SMALPs due to intercalated polymers reminiscent of detergent solubilization. This revelation not only casts doubt on the native nanodisc notion but also indicates that not all membrane proteins solubilized in SMALPs have the same supporting matrix. The utility of SMALPs or SMALP analogues in membrane biology will likely be compromised[87] if we fail to separate and identify the membrane-protein-carrying SMALPs of different structures. To highlight this concept, we demonstrate here that proteorhodopsin (PR), a light-driven proton pump,[88] solubilized in SMALPs is indeed embedded among different supporting matrices that entail different photocycle kinetics.

The proton-pumping photocycle of PR is characterized by a series of spectroscopically distinctive intermediate states. Although the exact kinetic model of PR is still under debate, its photocycle model was proposed[89] based on the kinetic model of bacteriorhodopsin.[90] Time-resolved visible spectros-

https://doi.org/10.1021/acs.biomac.3c00034
Biomacromolecules 2023, 24, 1819−1838

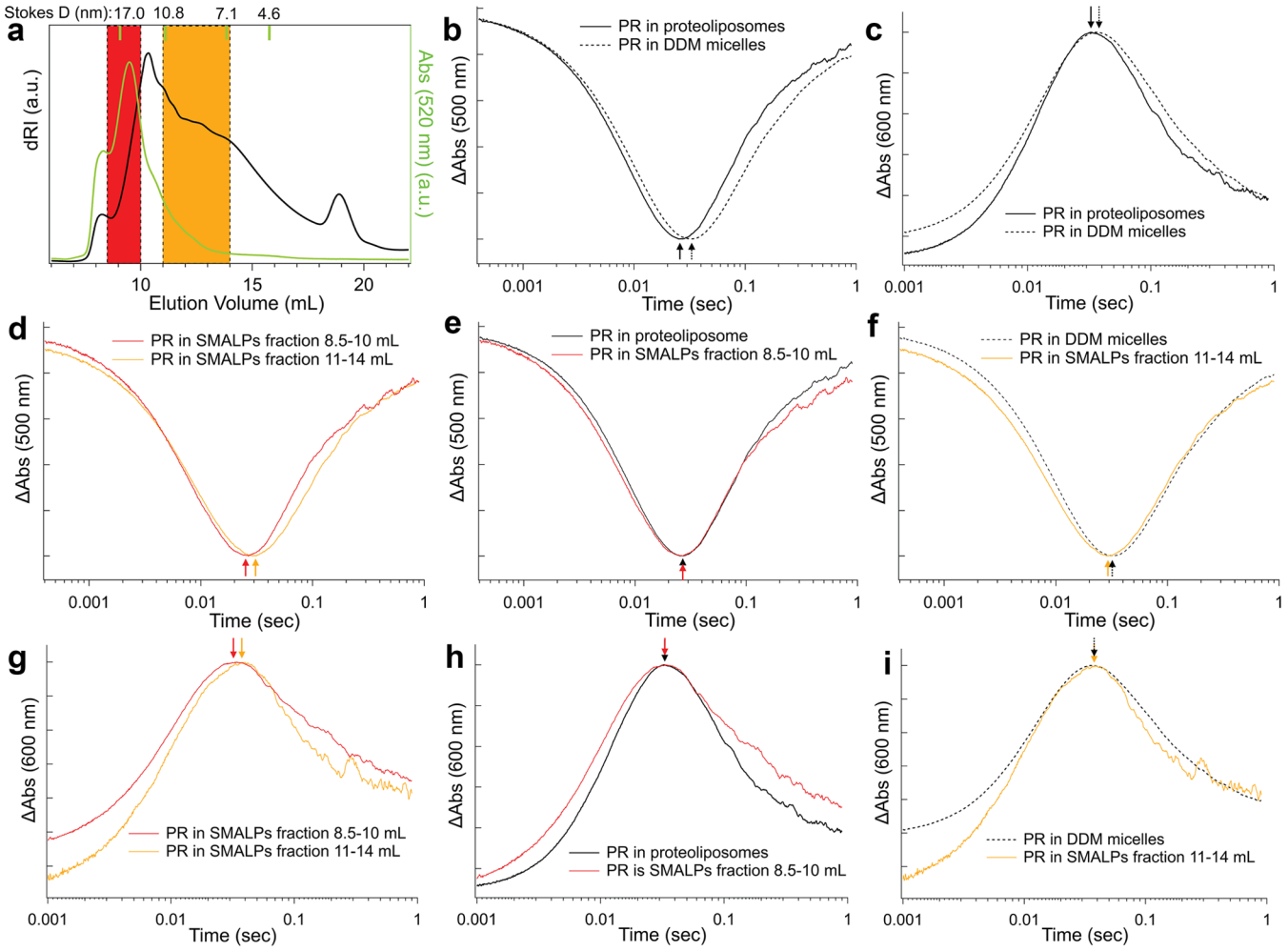

Figure 6. PR solubilized in different SMALP structures shows different proton-pumping photocycle kinetics. SMALPs were prepared by solubilizing proteoliposomes comprised of PR and DMPC with RAFT SMA-*m*. The same parent proteoliposomes and those solubilized by DDM micelles were used as controls. (a) SEC elution profiles of SMALPs (500 μL injection, prefiltered through a 0.2 μm filter) monitored by the RI (black trace) and UV-Vis (green trace) detectors, respectively, with protein markers run under the same configurations shown on the top. The UV-Vis detector monitored PR's retinal absorbance at 520 nm. The PR-carrying elution volumes were selectively collected into two fractions, as delineated by the dotted lines and denoted in red and yellow, respectively, that constitute mainly of SMA-remodeled proteoliposomes and SMA-encased LNDs. (b, c) As controls, flash photolysis of PR in proteoliposomes (solid black trace) and DDM micelles (dotted black trace) with its two characteristic photocycle intermediate states monitored at 500 nm (b) and 600 nm (c), respectively, shows that DDM solubilization decelerates the proton-pumping photocycle of PR. The peak absorbance change (ΔAbs) in proteoliposomes and DDM micelles, as marked by solid and dotted black arrows, respectively, clearly show the red-shift (i.e., increased time constant) of the bleaching of PR's dark parent state (b) and rising of its K and N/O intermediate states (c) as PR in proteoliposomes is solubilized by DDM. (d–i) Flash photolysis of PR carried in the two different SMALP fractions are also monitored at 500 nm (d–f) and 600 nm (g–i), respectively. The same color scheme in (a) is used to denote the two different SMALP structures. At each characteristic photocycle intermediate state, flash photolysis traces of the two SMALP structures are compared to each other (d, g) and individually compared to PR in proteoliposomes (e, h) and DDM micelles (f, i). The deceleration of PR's photocycle in SMA-encased LNDs (yellow trace) as compared to that in SMA-remodeled proteoliposomes (red trace) is in clear display (d, g). While the photocycle kinetics of PR in SMA-remodeled proteoliposomes is identical to that in proteoliposomes (e, h), the decelerated photocycle in SMA-encased LNDs approaches that of PR in DDM micelles (f, i).

copy (i.e., flash photolysis) that monitors the key photocycle steps of rhodopsins, including PR,[77,89,91−93] has been widely used to characterize their functions. As we reported before,[77] two important wavelengths indicative of PR's proton-pumping photocycle, i.e., 500 nm—bleaching of the dark parent state reporting on the overall photocycle turnover kinetics, and 600 nm—rising of the red-shifted K and N/O intermediates reporting on retinal isomerization and isomeric composition of the dark state, were monitored to compare PR function in different SMALP structures. The SMALPs were prepared by solubilizing proteoliposomes comprised of PR and DMPC with RAFT SMA-*m* at a *P*/*L* weight ratio of 3/1. As discussed earlier in Figure 2, the SEC profile of SMALPs can be roughly divided into three elution bands based on their hydrodynamic diameters, i.e., the L-, M-, and S-band, respectively, with the PR-carrying fractions (green trace) spanning a wide range of SMALP sizes (Figure 6a). Also as we discussed before, caution should be taken on the potential limitations of the specific detector used to monitor SEC elution. The completely different elution profiles revealed by UV-Vis (green trace) and RI detector (black trace) could explain the occasionally illusional interpretation of SMALPs based on one type of SEC detector, such as the claims of "homogeneous" or "monodisperse" SMALPs based on the single elution peak observed

https://doi.org/10.1021/acs.biomac.3c00034
Biomacromolecules 2023, 24, 1819−1838

by a UV-Vis detector. To demonstrate the heterogeneity of SMALPs and the concept that even SMALPs eluted under the same apparent peak revealed by the UV-Vis detector are not necessarily "monodisperse" or "homogeneous", we selectively collected two fractions of PR-carrying SMALPs at the beginning and middle of the M-band as indicated by the red and yellow zone, respectively (Figure 6a), both of which rest within the same one elution peak revealed by the UV-Vis detector but presumably constitute mainly of two different SMALP structures, i.e., SMA-remodeled proteoliposomes and SMA-encased LNDs, respectively, based on our earlier analysis (Figures 3 and 4). As controls, the photocycle kinetics of PR in the parent proteoliposomes before and after DDM solubilization were also monitored.

Like other membrane proteins,[82−84] the function of PR responds to the local milieu in which it is embedded, and its photocycle kinetics reflects how the supporting matrix affects conformational changes of PR.[77] Solubilization of PR-carrying proteoliposomes by DDM decelerates PR's photocycle, as seen in the red-shifted (i.e., increased time constant) flash photolysis traces of PR in DDM micelles (dotted black trace) as compared to PR in proteoliposomes (solid black trace) at 500 nm (Figure 6b) and 600 nm (Figure 6c), respectively, corresponding to the decelerated kinetics for both the bleaching of PR's dark parent state and rising of its K and N/O intermediate states. To visually aid the comparison, the peak absorbance change (ΔAbs) of PR in proteoliposomes and DDM micelles are marked by solid and dotted black arrows, respectively.

Interestingly, a similar decelerated photocycle of PR is also observed in PR-carrying SMALPs of decreasing sizes (i.e., increasing solubilization by SMA, see Figure 3). For the two SMALP fractions that presumably constitute mainly of SMA-remodeled proteoliposomes and SMA-encased LNDs collected at elution volumes 8.5−10 and 11−14 mL, respectively, the red-shifted flash photolysis traces of SMA-encased LNDs (yellow) as compared to SMA-remodeled proteoliposomes (red) are shown at both 500 nm (Figure 6d) and 600 nm (Figure 6g). Again, the peak absorbance change of PR is marked by arrows of the same color as their respective traces to visually aid the comparison. To put the decelerated photocycle of PR in context, we compared the flash photolysis traces of PR in SMA-remodeled proteoliposomes (red) with that of parent proteoliposomes (black) at both 500 nm (Figure 6e) and 600 nm (Figure 6h), and the flash photolysis traces of PR in SMA-encased LNDs (yellow) with PR in DDM micelles (dotted black) at both 500 nm (Figure 6f) and 600 nm (Figure 6i) as well. We found that the photocycle kinetics of PR in SMA-remodeled proteoliposomes is identical to that in the parent proteoliposomes (Figure 6e,h). This observation once again confirmed our earlier assessment (Figures 3 and 4) that SMALPs eluted at the beginning of the M-band in SEC are essentially SMA-remodeled liposomal structures with low concentrations of doped copolymers that have not reached the point of membrane solubilization, such that the local membrane milieu surrounding PR remains nearly unchanged, so does its proton-pumping photocycle. On the contrary, SMALPs eluted in the middle of the M-band in SEC were shown to be solubilized membrane fragments comprised primarily of SMA-encased LNDs (Figures 3 and 4) characterized by higher concentrations of copolymers intercalated into both the hydrophobic edge and hydrophilic surface of the LNDs, as illustrated in Figure 4j. The copolymer intercalations ease lipid−lipid interactions and lower the lipid gel-to-liquid crystalline transition temperature (Figure 4) in a way reminiscent of detergent solubilization (Figure S6, SI). Not surprisingly, we observed the decelerated photocycle of PR in SMA-encased LNDs that resembles closely the photocycle of PR in DDM micelles (Figure 6f,i), underscoring the similar effect on membrane disruption between SMA and detergent solubilization. Like the lipidomic study that revealed the altered lipid composition in SMALPs,[67] the membrane disruption by SMA doping is also inconducive to the putative native nanodisc notion of SMALPs.

CONCLUSIONS

In summary, synthetic SMA or SMA-like copolymers are powerful tools in membrane biology because of their unique ability to extract membrane proteins directly from cell membranes that bypasses the often-disruptive detergent solubilization process. Notwithstanding their great potential, cautions should be taken on the nanodiscs or native nanodiscs notion of SMALPs or SMALP analogues because the amphipathic copolymers themselves can behave much like detergent (i.e., polymer surfactant) depending on their amphiphilic balances. We demonstrated here unambiguously the heterogeneity of SMALPs manifested by a variety of polymer-solubilized states with different degrees of polymer−lipid intermixing, among which the polymer-encased nanodisc is one possibility but not the only one. The population distribution of different SMALP components responds not only to SMA or SMA-like copolymers of different structures but also the overall P/L weight ratio in the self-assembly system. We attributed the structural heterogeneity of SMALPs to the inevitable microstructure variations among synthetic SMA copolymer chains in size, sequence, and hydrophobic/hydrophilic ratio that result in their polydisperse amphiphilic balance and detergency, which in turn help dictate their different modes of interaction on remodeling membranes.

Unfortunately, the heterogeneous nature of SMALPs and SMALP analogues has been largely overlooked in previous reports. Although attempts have been made occasionally to remove large self-assembled components by centrifugation at empirical speeds (e.g., 20,000g for 30 min,[63] 21,000g for 1 h,[66] or 140,000g for 1 h,[79] etc.) or remove both large aggregates and excess copolymers by SEC,[60] it has not been recognized yet that even the putative "nanodisc" products in the typical size range of ∼5−25 nm are in fact a mixture of a wide range of polymer-solubilized structures, among which polymer-remodeled (proteo)liposomes, polymer-encased LNDs, polymer−lipid mixed micelles, and an array of intermediate structures in-between with different degrees of polymer−lipid intermixing may exist. Separation and purification methods such as SEC should be part of the standard protocol in the preparation of polymer-encased nanodiscs for use in membrane biology. Unless the nanodisc fraction is purified and explicitly verified, we recommend referring to the polymer-solubilized membranes as "xx-lipid particles" ("xx" stands for the name of the amphipathic copolymer being used) following the SMALP term originally coined by Overduin and colleagues.[24] The blanket interpretation of any as-prepared polymer-solubilized membrane as "nanodisc" or even "native nanodisc" is rather misleading in our opinion.

In addition, because of the inherent structural heterogeneity in polymer-solubilized membranes, a given membrane protein extracted by amphipathic copolymers may rest in a number of

https://doi.org/10.1021/acs.biomac.3c00034
Biomacromolecules 2023, 24, 1819−1838

different polymer-solubilized states with very different local supporting milieu, which may give rise to the structural and functional inhomogeneity of the embedded membrane protein. Not only could the lipid composition in its local milieu differ from each other and from that in the parent membranes,[67] the lipid−lipid or lipid−protein interactions could also be altered due to polymer intercalations. To highlight this important concept, we demonstrated that PR solubilized by the same SMALP preparation is embedded among different polymer−lipid co-assembled states that entail different photocycle kinetics. A recent study by Morrison et al. also showed that membrane protein extracted in SMALPs might lose activity altogether,[87] likely caused by the altered local supporting milieu of the protein due to polymer intercalations. It is thus rather risky to take for granted that polymer-solubilized membranes are by default native nanodiscs. Detergent-free extraction of membrane proteins directly from native membranes by SMA or SMA-like copolymers does not guarantee the "nativeness" of the supporting matrices in which the proteins are embedded because the copolymers themselves could behave just like detergents depending on their amphiphilic balances and detergency. Structural and functional studies of membrane proteins extracted in SMALPs or SMALP analogues would benefit from separation, purification, and identification of the specific polymer−lipid structures in which the proteins are carried.

Furthermore, we demonstrated that some of the most often used methods in previous reports to validate the formation of LNDs, such as DLS, TEM, DSC, and ^{31}P-NMR, have their limits. While those methods are powerful in revealing membrane solubilization, they fall short of telling whether the solubilized membranes truly become nanodiscs. This challenge is exacerbated when a wide variety of different structures co-exist in the solubilized membranes. We showed that separation of the different self-assembled structures is key for meaningful comparison and characterization of the polymer-solubilized membranes formed under different conditions, and the P/L stoichiometric ratios of individual SMALP fractions offer unwavering insight to explicate their respective structures. For amphipathic copolymers with poorly defined chain sizes that prevent quantitative determination of the P/L stoichiometric ratios, the separation of the different polymer-solubilized structures still simplifies structural characterization by the abovementioned methods. Fractionation of the different SMALP products by sizes helps create more structurally homogeneous samples for other methods such as small-angle X-ray or neutron scattering, cryoEM, and biological activity assays of the membrane proteins to be applied to dissect the different self-assembled structures in SMALPs and SMALP analogues.

Finally, we are cautiously optimistic that innovative polymerization approaches can be developed to synthesize amphipathic MSPols with well-defined microstructures, which will give rise to their nearly uniform amphiphilic balance and detergency apt to partition biomembranes into "native-like" nanodiscs. Toward that end, it is imperative to elucidate the structure−activity relationship of membrane solubilization using rationally designed model copolymers of well-defined structures. Separation and identification of the different self-assembled structures in SMALPs and SMALP analogues would be the first important step on this long journey.

■ ASSOCIATED CONTENT

Supporting Information

The Supporting Information is available free of charge at https://pubs.acs.org/doi/10.1021/acs.biomac.3c00034.

Additional data on the synthesis and characterization of SMA copolymers and SMALPs (PDF)

■ AUTHOR INFORMATION

Corresponding Author

Hongjun Liang − *Department of Cell Physiology & Molecular Biophysics, Center for Membrane Protein Research, School of Medicine, Texas Tech University Health Sciences Center, Lubbock, Texas 79430, United States;* orcid.org/0000-0003-0864-9106; Email: H.liang@ttuhsc.edu

Authors

Elizabeth Kamilar − *Department of Cell Physiology & Molecular Biophysics, Center for Membrane Protein Research, School of Medicine, Texas Tech University Health Sciences Center, Lubbock, Texas 79430, United States*

Jitender Bariwal − *Department of Cell Physiology & Molecular Biophysics, Center for Membrane Protein Research, School of Medicine, Texas Tech University Health Sciences Center, Lubbock, Texas 79430, United States*

Wan Zheng − *Department of Cell Physiology & Molecular Biophysics, Center for Membrane Protein Research, School of Medicine, Texas Tech University Health Sciences Center, Lubbock, Texas 79430, United States*

Hairong Ma − *Department of Cell Physiology & Molecular Biophysics, Center for Membrane Protein Research, School of Medicine, Texas Tech University Health Sciences Center, Lubbock, Texas 79430, United States*

Complete contact information is available at: https://pubs.acs.org/10.1021/acs.biomac.3c00034

Author Contributions

H.L. supervised the project. E.K., J.B., and H.M. conceived the experimental plan and developed methods. J.B. and W.Z. performed polymer synthesis and characterization. E.K. performed SMALP synthesis and characterization. H.M. performed flash photolysis characterization and SMALP characterization. All authors contributed to data analysis. This manuscript was written through contributions of all authors. All authors have given approval to the final version of the manuscript.

Notes

The authors declare no competing financial interest.

■ ACKNOWLEDGMENTS

The authors appreciate the generous gift of Lipodisq SMAs from Dr. Steve Tonge, Managing Director of Malvern Cosmeceutics Ltd. This work was supported in part by the NSF grants DMR-2213969 and DMR-1810767.

■ ABBREVIATIONS

SMA, styrene-maleic acid copolymer; SMAnh, styrene-maleic anhydride copolymer; SMALP, SMA/lipid particle; DIBMAP, diisobutylene-maleic acid lipid particle; RAFT, reversible addition−fragmentation chain transfer; MSP, membrane-scaffold proteins; MSPol, membrane-scaffold polymers; LND, lipid nanodisc; SAXS, small-angle X-ray scattering; AFM,

https://doi.org/10.1021/acs.biomac.3c00034
Biomacromolecules 2023, 24, 1819−1838

atomic force microscopy; TEM, transmission electron microscopy; DLS, dynamic light scattering; DSC, differential scanning calorimetry; SEC, size-exclusion chromatography; NMR, nuclear magnetic resonance spectroscopy; FT-IR, Fourier transform infrared spectroscopy; DMPC, 1,2-dimyristoyl-*sn*-glycero-3-phosphocholine; DDM, *n*-dodecyl-*β*-D-maltoside

REFERENCES

(1) Sackmann, E. Supported membranes: Scientific and practical applications. *Science* **1996**, *271*, 43−48.
(2) Allen, T. M.; Cullis, P. R. Liposomal drug delivery systems: From concept to clinical applications. *Adv. Drug Delivery Rev.* **2013**, *65*, 36−48.
(3) Brinkhuis, R. P.; Rutjes, F.; van Hest, J. C. M. Polymeric vesicles in biomedical applications. *Polym. Chem.* **2011**, *2*, 1449−1462.
(4) Castellana, E. T.; Cremer, P. S. Solid supported lipid bilayers: From biophysical studies to sensor design. *Surf. Sci. Rep.* **2006**, *61*, 429−444.
(5) Jonas, A.[32] Reconstitution of high-density-lipoproteins. In *Methods in Enzymology*; Elsevier, 1986; Vol. *128*, pp 553−582.
(6) Bayburt, T. H.; Grinkova, Y. V.; Sligar, S. G. Self-Assembly of Discoidal Phospholipid Bilayer Nanoparticles with Membrane Scaffold Proteins. *Nano Lett.* **2002**, *2*, 853−856.
(7) Denisov, I. G.; Grinkova, Y. V.; Lazarides, A. A.; Sligar, S. G. Directed self-assembly of monodisperse phospholipid bilayer nanodiscs with controlled size. *J. Am. Chem. Soc.* **2004**, *126*, 3477−3487.
(8) Denisov, I. G.; Sligar, S. G. Nanodiscs for structural and functional studies of membrane proteins. *Nat. Struct. Mol. Biol.* **2016**, *23*, 481−486.
(9) Denisov, I. G.; Sligar, S. G. Nanodiscs in Membrane Biochemistry and Biophysics. *Chem. Rev.* **2017**, *117*, 4669−4713.
(10) Yokogawa, M.; Fukuda, M.; Osawa, M. Nanodiscs for Structural Biology in a Membranous Environment. *Chem. Pharm. Bull.* **2019**, *67*, 321−326.
(11) Gardill, B.; Huang, J.; Tu, L.; Van Petegem, F.; Oxenoid, K.; Thomson, C. A. Nanodisc technology facilitates identification of monoclonal antibodies targeting multi-pass membrane proteins. *Sci. Rep.* 2020, *10* (1), 1130.
(12) Duivenvoorden, R.; Tang, J.; Cormode, D. P.; Mieszawska, A. J.; Izquierdo-Garcia, D.; Ozcan, C.; Otten, M. J.; Zaidi, N.; Lobatto, M. E.; van Rijs, S. M.; et al. A statin-loaded reconstituted high-density lipoprotein nanoparticle inhibits atherosclerotic plaque inflammation. *Nat. Commun.* **2014**, *5*, No. 3531.
(13) Fischer, N. O.; Rasley, A.; Corzett, M.; Hwang, M. H.; Hoeprich, P. D.; Blanchette, C. D. Colocalized Delivery of Adjuvant and Antigen Using Nanolipoprotein Particles Enhances the Immune Response to Recombinant Antigens. *J. Am. Chem. Soc.* **2013**, *135*, 2044−2047.
(14) Jomard, A.; Osto, E. High Density Lipoproteins: Metabolism, Function, and Therapeutic Potential. *Front. Cardiovasc. Med.* **2020**, *7*, 39.
(15) Bhattacharya, P.; Grimme, S.; Ganesh, B.; Gopisetty, A.; Sheng, J. R.; Martinez, O.; Jayarama, S.; Artinger, M.; Meriggioli, M.; Prabhakar, B. S. Nanodisc-Incorporated Hemagglutinin Provides Protective Immunity against Influenza Virus Infection. *J. Virol.* **2010**, *84*, 361−371.
(16) Huang, C.-H.; Zhang, Z.-Y.; Shi, Y.-F.; Hua, Q.; Wei, P. Research Progress of Nanodiscs in Biomedical Field. *Prog. Biochem. Biophys.* **2020**, *47*, 1250−1260.
(17) Bavishi, K.; Laursen, T.; Martinez, K. L.; Moller, B. L.; Della Pia, E. A. Application of nanodisc technology for direct electrochemical investigation of plant cytochrome P450s and their NADPH P450 oxidoreductase. *Sci. Rep.* **2016**, *6*, No. 29459.
(18) Glück, J. M.; Koenig, B. W.; Willbold, D. Nanodiscs allow the use of integral membrane proteins as analytes in surface plasmon resonance studies. *Anal. Biochem.* **2011**, *408*, 46−52.
(19) Lu, Y.; Zhang, H.; Niedzwiedzki, D. M.; Jiang, J.; Blankenship, R. E.; Gross, M. L. Fast Photochemical Oxidation of Proteins Maps the Topology of Intrinsic Membrane Proteins: Light-Harvesting Complex 2 in a Nanodisc. *Anal. Chem.* **2016**, *88*, 8827−8834.
(20) Wang, P.; Chang, A. Y.; Novosad, V.; Chupin, V. V.; Schaller, R. D.; Rozhkova, E. A. Cell-Free Synthetic Biology Chassis for Nanocatalytic Photon-to-Hydrogen Conversion. *ACS Nano* **2017**, *11*, 6739−6745.
(21) Lyons, J. A.; Boggild, A.; Nissen, P.; Frauenfeld, J. Saposin-Lipoprotein Scaffolds for Structure Determination of Membrane Transporters. In *Methods in Enzymology*; Ziegler, C., Ed.; A Structure-Function Toolbox for Membrane Transporter and Channels; Elsevier Academic Press: Cambridge, MA, 2017; Vol. *594*, pp 85−99.
(22) Pan, J. J.; Dalzini, A.; Khadka, N. K.; Aryal, C. M.; Song, L. K. Lipid Extraction by alpha-Synuclein Generates Semi-Transmembrane Defects and Lipoprotein Nanoparticles. *ACS Omega* **2018**, *3*, 9586−9597.
(23) Zhao, Z.; Zhang, M.; Hogle, J. M.; Shih, W. M.; Wagner, G.; Nasr, M. L. DNA-Corralled Nanodiscs for the Structural and Functional Characterization of Membrane Proteins and Viral Entry. *J. Am. Chem. Soc.* **2018**, *140*, 10639−10643.
(24) Knowles, T. J.; Finka, R.; Smith, C.; Lin, Y. P.; Dafforn, T.; Overduin, M. Membrane proteins solubilized intact in lipid containing nanoparticles bounded by styrene maleic acid copolymer. *J. Am. Chem. Soc.* **2009**, *131*, 7484−7485.
(25) Fiori, M. C.; Jiang, Y. J.; Altenberg, G. A.; Liang, H. J. Polymer-encased nanodiscs with improved buffer compatibility. *Sci. Rep.* **2017**, *7*, No. 7432.
(26) Oluwole, A. O.; Klingler, J.; Danielczak, B.; Babalola, J. O.; Vargas, C.; Pabst, G.; Keller, S. Formation of Lipid-Bilayer Nanodiscs by Diisobutylene/Maleic Acid (DIBMA) Copolymer. *Langmuir* **2017**, *33*, 14378−14388.
(27) Yasuhara, K.; Arakida, J.; Ravula, T.; Ramadugu, S. K.; Sahoo, B.; Kikuchi, J.; Ramamoorthy, A. Spontaneous Lipid Nanodisc Formation by Amphiphilic Polymethacrylate Copolymers. *J. Am. Chem. Soc.* **2017**, *139*, 18657−18663.
(28) Ravula, T.; Hardin, N. Z.; Di Mauro, G. M.; Ramamoorthy, A. Styrene maleic acid derivates to enhance the applications of bio-inspired polymer based lipid-nanodiscs. *Eur. Polym. J.* **2018**, *108*, 597−602.
(29) Matsuoka, H. Polymer Surfactant. In *Encyclopedia of Polymeric Nanomaterials*; Kobayashi, S.; Müllen, K., Eds.; Springer Berlin Heidelberg, 2015; pp 1917−1922.
(30) Raffa, P.; Wever, D. A. Z.; Picchioni, F.; Broekhuis, A. A. Polymeric Surfactants: Synthesis, Properties, and Links to Applications. *Chem. Rev.* **2015**, *115*, 8504−8563.
(31) Tribet, C.; Audebert, R.; Popot, J. L. Amphipols: Polymers that keep membrane proteins soluble in aqueous solutions. *Proc. Natl. Acad. Sci. U.S.A.* **1996**, *93*, 15047−15050.
(32) Popot, J. L.; Berry, E. A.; Charvolin, D.; Creuzenet, C.; Ebel, C.; Engelman, D. M.; Flotenmeyer, M.; Giusti, F.; Gohon, Y.; Herve, P.; et al. Amphipols: polymeric surfactants for membrane biology research. *Cell. Mol. Life Sci.* **2003**, *60*, 1559−1574.
(33) Ladavière, C.; Toustou, M.; Gulik-Krzywicki, T.; Tribet, C. Slow reorganization of small phosphatidylcholine vesicles upon adsorption of amphiphilic polymers. *J. Colloid Interface Sci.* **2001**, *241*, 178−187.
(34) Vial, F.; Rabhi, S.; Tribet, C. Association of octyl-modified poly(acrylic acid) onto unilamellar vesicles of lipids and kinetics of vesicle disruption. *Langmuir* **2005**, *21*, 853−862.
(35) Murakami, T. Phospholipid nanodisc engineering for drug delivery systems. *Biotechnol. J.* **2012**, *7*, 762−767.
(36) Marie, E.; Sagan, S.; Cribier, S.; Tribet, C. Amphiphilic Macromolecules on Cell Membranes: From Protective Layers to Controlled Permeabilization. *J. Membr. Biol.* **2014**, *247*, 861−881.
(37) Tribet, C.; Vial, F. Flexible macromolecules attached to lipid bilayers: impact on fluidity, curvature, permeability and stability of the membranes. *Soft Matter* **2008**, *4*, 68−81.

https://doi.org/10.1021/acs.biomac.3c00034
Biomacromolecules 2023, 24, 1819−1838

(38) Scott, R. W.; DeGrado, W. F.; Tew, G. N. *De novo* designed synthetic mimics of antimicrobial peptides. *Curr. Opin. Biotechnol.* **2008**, *19*, 620−627.
(39) Tew, G. N.; Scott, R. W.; Klein, M. L.; Degrado, W. F. *De novo* design of antimicrobial polymers, foldamers, and small molecules: From discovery to practical applications. *Acc. Chem. Res.* **2010**, *43*, 30−39.
(40) Borden, K. A.; Eum, K. M.; Langley, K. H.; Tan, J. S.; Tirrell, D. A.; Voycheck, C. L. pH-Dependent Vesicle-to-Micelle Transition in an Aqueous Mixture of Dipalmitoylphosphatidylcholine and a Hydrophobic Polyelectrolyte. *Macromolecules* **1988**, *21*, 2649−2651.
(41) Chung, J. C.; Gross, D. J.; Thomas, J. L.; Tirrell, D. A.; OpsahlOng, L. R. pH-Sensitive, cation-selective channels formed by a simple synthetic polyelectrolyte in artificial bilayer membranes. *Macromolecules* **1996**, *29*, 4636−4641.
(42) Maeda, H. SMANCS and Polymer-Conjugated Macromolecular Drugs - Advantages In Cancer-Chemotherapy. *Adv. Drug Delivery Rev.* **1991**, *6*, 181−202.
(43) Henry, S. M.; El-Sayed, M. E. H.; Pirie, C. M.; Hoffman, A. S.; Stayton, P. S. pH-responsive poly(styrene-alt-maleic anhydride) alkylamide copolymers for intracellular drug delivery. *Biomacromolecules* **2006**, *7*, 2407−2414.
(44) Tonge, S. R.; Tighe, B. J. Responsive hydrophobically associating polymers: a review of structure and properties. *Adv. Drug Delivery Rev.* **2001**, *53*, 109−122.
(45) Barniol-Xicota, M.; Verhelst, S. H. L. Stable and Functional Rhomboid Proteases in Lipid Nanodiscs by Using Diisobutylene/Maleic Acid Copolymers. *J. Am. Chem. Soc.* **2018**, *140*, 14557−14561.
(46) Danielczak, B.; Keller, S. Lipid exchange among polymer-encapsulated nanodiscs by time-resolved Forster resonance energy transfer. *Methods* **2020**, *180*, 27−34.
(47) Dominguez Pardo, J. J.; Dorr, J. M.; Renne, M. F.; Ould-Braham, T.; Koorengevel, M. C.; van Steenbergen, M. J.; Killian, J. A. Thermotropic properties of phosphatidylcholine nanodiscs bounded by styrene-maleic acid copolymers. *Chem. Phys. Lipids* **2017**, *208*, 58−64.
(48) Grethen, A.; Oluwole, A. O.; Danielczak, B.; Vargas, C.; Keller, S. Thermodynamics of nanodisc formation mediated by styrene/maleic acid (2:1) copolymer. *Sci. Rep.* **2017**, *7*, No. 11517.
(49) Lindhoud, S.; Carvalho, V.; Pronk, J. W.; Aubin-Tam, M. E. SMA-SH: Modified Styrene-Maleic Acid Copolymer for Functionalization of Lipid Nanodiscs. *Biomacromolecules* **2016**, *17*, 1516−1522.
(50) Oluwole, A. O.; Danielczak, B.; Meister, A.; Babalola, J. O.; Vargas, C.; Keller, S. Solubilization of Membrane Proteins into Functional Lipid-Bilayer Nanodiscs Using a Diisobutylene/Maleic Acid Copolymer. *Angew. Chem. Int. Ed.* **2017**, *56*, 1919−1924.
(51) Ravula, T.; Hardin, N. Z.; Ramadugu, S. K.; Cox, S. J.; Ramamoorthy, A. Formation of pH-Resistant Monodispersed Polymer-Lipid Nanodiscs. *Angew. Chem., Int. Ed.* **2018**, *57*, 1342−1345.
(52) Ravula, T.; Ramadugu, S. K.; Di Mauro, G.; Ramamoorthy, A. Bioinspired, Size-Tunable Self-Assembly of Polymer-Lipid Bilayer Nanodiscs. *Angew. Chem., Int. Ed.* **2017**, *56*, 11466−11470.
(53) Ravula, T.; Ramamoorthy, A. Synthesis, Characterization, and Nanodisc Formation of Non-ionic. *Polymers. Angew. Chem., Int. Ed.* **2021**, *60*, 16885−16888.
(54) Bersch, B.; Dorr, J. M.; Hessel, A.; Killian, J. A.; Schanda, P. Proton-Detected Solid-State NMR Spectroscopy of a Zinc Diffusion Facilitator Protein in Native Nanodiscs. *Angew. Chem., Int. Ed.* **2017**, *56*, 2508−2512.
(55) Dörr, J. M.; Koorengevel, M. C.; Schafer, M.; Prokofyev, A. V.; Scheidelaar, S.; van der Cruijsen, E. A. W.; Dafforn, T. R.; Baldus, M.; Killian, J. A. Detergent-free isolation, characterization, and functional reconstitution of a tetrameric K+ channel: The power of native nanodiscs. *Proc. Natl. Acad. Sci. U.S.A.* **2014**, *111*, 18607−18612.
(56) Esmaili, M.; Tancowny, B. P.; Wang, X. Y.; Moses, A.; Cortez, L. M.; Sim, V. L.; Wille, H.; Overduin, M. Native nanodiscs formed by styrene maleic acid copolymer derivatives help recover infectious prion multimers bound to brain-derived lipids. *J. Biol. Chem.* **2020**, *295*, 8460−8469.
(57) Overduin, M.; Esmaili, M. Native Nanodiscs and the Convergence of Lipidomics, Metabolomics, Interactomics and Proteomics. *Appl. Sci.* **2019**, *9*, 1230.
(58) Smirnova, I. A.; Sjostrand, D.; Li, F.; Bjorck, M.; Schafer, J.; Ostbye, H.; Hogbom, M.; von Ballmoos, C.; Lander, G. C.; Adelroth, P.; Brzezinski, P. Isolation of yeast complex IV in native lipid nanodiscs. *Biochim. Biophys. Acta, Biomembr.* **2016**, *1858*, 2984−2992.
(59) Lee, S. C.; Knowles, T. J.; Postis, V. L. G.; Jamshad, M.; Parslow, R. A.; Lin, Y. P.; Goldman, A.; Sridhar, P.; Overduin, M.; Muench, S. P.; Dafforn, T. R. A method for detergent-free isolation of membrane proteins in their local lipid environment. *Nat. Protoc.* **2016**, *11*, 1149−1162.
(60) Hall, S. C. L.; Tognoloni, C.; Price, G. J.; Klumperman, B.; Edler, K. J.; Dafforn, T. R.; Arnold, T. Influence of Poly(styrene-co-maleic acid) Copolymer Structure on the Properties and Self-Assembly of SMALP Nanodiscs. *Biomacromolecules* **2018**, *19*, 761−772.
(61) Scheidelaar, S.; Koorengevel, M. C.; van Walree, C. A.; Dominguez, J. J.; Dorr, J. M.; Killian, J. A. Effect of Polymer Composition and pH on Membrane Solubilization by Styrene-Maleic Acid Copolymers. *Biophys. J.* **2016**, *111*, 1974−1986.
(62) Craig, A. F.; Clark, E. E.; Sahu, I. D.; Zhang, R. F.; Frantz, N. D.; Al-Abdul-Wahid, M. S.; Dabney-Smith, C.; Konkolewicz, D.; Lorigan, G. A. Tuning the size of styrene-maleic acid copolymer-lipid nanoparticles (SMALPs) using RAFT polymerization for biophysical studies. *Biochim. Biophys. Acta, Biomembr.* **2016**, *1858*, 2931−2939.
(63) Smith, A. A. A.; Autzen, H. E.; Laursen, T.; Wu, V.; Yen, M.; Hall, A.; Hansen, S. D.; Cheng, Y. F.; Xu, T. Controlling Styrene Maleic Acid Lipid Particles through RAFT. *Biomacromolecules* **2017**, *18*, 3706−3713.
(64) Morrison, K. A.; Akram, A.; Mathews, A.; Khan, Z. A.; Patel, J. H.; Zhou, C. M.; Hardy, D. J.; Moore-Kelly, C.; Patel, R.; Odiba, V.; et al. Membrane protein extraction and purification using styrene-maleic acid (SMA) copolymer: effect of variations in polymer structure. *Biochem. J.* **2016**, *473*, 4349−4360.
(65) Domínguez Pardo, J. J.; Koorengevel, M. C.; Uwugiaren, N.; Weijers, J.; Kopf, A. H.; Jahn, H.; van Walree, C. A.; van Steenbergen, M. J.; Killian, J. A. Membrane Solubilization by Styrene-Maleic Acid Copolymers: Delineating the Role of Polymer Length. *Biophys. J.* **2018**, *115*, 129−138.
(66) Cunningham, R. D.; Kopf, A. H.; Elenbaas, B. O. W.; Staal, B. B. P.; Pfukwa, R.; Killian, J. A.; Klumperman, B. Iterative RAFT-Mediated Copolymerization of Styrene and Maleic Anhydride toward Sequence- and Length-Controlled Copolymers and Their Applications for Solubilizing Lipid Membranes. *Biomacromolecules* **2020**, *21*, 3287−3300.
(67) Barniol-Xicota, M.; Verhelst, S. H. L. Lipidomic and in-gel analysis of maleic acid co-polymer nanodiscs reveals differences in composition of solubilized membranes. *Commun. Biol.* **2021**, *4*, No. 218.
(68) Bjørnestad, V. A.; Orwick-Rydmark, M.; Lund, R. Understanding the Structural Pathways for Lipid Nanodisc Formation: How Styrene Maleic Acid Copolymers Induce Membrane Fracture and Disc Formation. *Langmuir* **2021**, *37*, 6178−6188.
(69) Jamshad, M.; Grimard, V.; Idini, I.; Knowles, T. J.; Dowle, M. R.; Schofield, N.; Sridhar, P.; Lin, Y. P.; Finka, R.; Wheatley, M.; et al. Structural analysis of a nanoparticle containing a lipid bilayer used for detergent-free extraction of membrane proteins. *Nano Res.* **2015**, *8*, 774−789.
(70) Belrhali, H.; Nollert, P.; Royant, A.; Menzel, C.; Rosenbusch, J. P.; Landau, E. M.; Pebay-Peyroula, E. Protein, lipid and water organization in bacteriorhodopsin crystals: a molecular view of the purple membrane at 1.9 Å resolution. *Structure* **1999**, *7*, 909−917.
(71) Vinothkumar, K. R. Structure of Rhomboid Protease in a Lipid Environment. *J. Mol. Biol.* **2011**, *407*, 232−247.

https://doi.org/10.1021/acs.biomac.3c00034
Biomacromolecules 2023, 24, 1819−1838

(72) Lai, J. T.; Filla, D.; Shea, R. Functional Polymers from Novel Carboxyl-Terminated Trithiocarbonates as Highly Efficient RAFT Agents. *Macromolecules* **2002**, *35*, 6754−6756.
(73) Fiori, M. C.; Zheng, W.; Kamilar, E.; Simiyu, G.; Altenberg, G. A.; Liang, H. J. Extraction and reconstitution of membrane proteins into lipid nanodiscs encased by zwitterionic styrene-maleic amide copolymers. *Sci. Rep.* **2020**, *10*, No. 9940.
(74) Davis, K. A.; Matyjaszewski, K. Atom transfer radical polymerization of tert-butyl acrylate and preparation of block copolymers. *Macromolecules* **2000**, *33*, 4039−4047.
(75) Jiang, Y.; Zheng, W.; Tran, K.; Kamilar, E.; Bariwal, J.; Ma, H.; Liang, H. Hydrophilic nanoparticles that kill bacteria while sparing mammalian cells reveal the antibiotic role of nanostructures. *Nat. Commun.* **2022**, *13*, No. 197.
(76) Goddard, A. D.; Dijkman, P. M.; Adamson, R. J.; dos Reis, R. I.; Watts, A. Reconstitution of Membrane Proteins: A GPCR as an Example. In *Methods in Enzymology*, 556th ed.; Shukla, A. K., Ed.; Elsevier Academic Press: Cambridge, MA, 2015; pp 405−424.
(77) Kuang, L. J.; Fernandes, D. A.; O'Halloran, M.; Zheng, W.; Jiang, Y. J.; Ladizhansky, V.; Brown, L. S.; Liang, H. J. "Frozen" block copolymer nanomembranes with light-driven proton pumping performance. *ACS Nano* **2014**, *8*, 537−545.
(78) Sanayei, R. A.; Odriscoll, K. F.; Klumperman, B. Pulsed-Laser Copolymerization of Styrene and Maleic Anhydride. *Macromolecules* **1994**, *27*, 5577−5582.
(79) Schmidt, V.; Sturgis, J. N. Modifying styrene-maleic acid copolymer for studying lipid nanodiscs. *Biochim. Biophys. Acta, Biomembr.* **2018**, *1860*, 777−783.
(80) Kučerka, N.; Liu, Y. F.; Chu, N. J.; Petrache, H. I.; Tristram-Nagle, S. T.; Nagle, J. F. Structure of fully hydrated fluid phase DMPC and DLPC lipid bilayers using X-ray scattering from oriented multilamellar arrays and from unilamellar vesicles. *Biophys. J.* **2005**, *88*, 2626−2637.
(81) Shaw, A. W.; McLean, M. A.; Sligar, S. G. Phospholipid phase transitions in homogeneous nanometer scale bilayer discs. *FEBS Lett.* **2004**, *556*, 260−264.
(82) Seddon, A. M.; Curnow, P.; Booth, P. J. Membrane proteins, lipids and detergents: not just a soap opera. *Biochim. Biophys. Acta, Biomembr.* **2004**, *1666*, 105−117.
(83) Sonntag, Y.; Musgaard, M.; Olesen, C.; Schiøtt, B.; Møller, J. V.; Nissen, P.; Thøgersen, L. Mutual adaptation of a membrane protein and its lipid bilayer during conformational changes. *Nat. Commun.* **2011**, *2*, No. 304.
(84) Zoonens, M.; Comer, J.; Masscheleyn, S.; Pebay-Peyroula, E.; Chipot, C.; Miroux, B.; Dehez, F. Dangerous Liaisons between Detergents and Membrane Proteins. The Case of Mitochondrial Uncoupling Protein 2. *J. Am. Chem. Soc.* **2013**, *135*, 15174−15182.
(85) Brown, C. J.; Trieber, C.; Overduin, M. Structural biology of endogenous membrane protein assemblies in native nanodiscs. *Curr. Opin. Struct. Biol.* **2021**, *69*, 70−77.
(86) Simon, K. S.; Pollock, N. L.; Lee, S. C. Membrane protein nanoparticles: the shape of things to come. *Biochem. Soc. Trans.* **2018**, *46*, 1495−1504.
(87) Morrison, K. A.; Wood, L.; Edler, K. J.; Doutch, J.; Price, G. J.; Koumanov, F.; Whitley, P. Membrane extraction with styrene-maleic acid copolymer results in insulin receptor autophosphorylation in the absence of ligand. *Sci. Rep.* **2022**, *12*, No. 3532.
(88) Béjà, O.; Spudich, E. N.; Spudich, J. L.; Leclerc, M.; DeLong, E. F. Proteorhodopsin phototrophy in the ocean. *Nature* **2001**, *411*, 786−789.
(89) Friedrich, T.; Geibel, S.; Kalmbach, R.; Chizhov, I.; Ataka, K.; Heberle, J.; Engelhard, M.; Bamberg, E. Proteorhodopsin is a light-driven proton pump with variable vectoriality. *J. Mol. Biol.* **2002**, *321*, 821−838.
(90) Lanyi, J. K.; Varo, G. The photocycles of bacteriorhodopsin. *Isr. J. Chem.* **1995**, *35*, 365−385.
(91) Dioumaev, A. K.; Brown, L. S.; Shih, J.; Spudich, E. N.; Spudich, J. L.; Lanyi, J. K. Proton transfers in the photochemical reaction cycle of proteorhodopsin. *Biochemistry* **2002**, *41*, 5348−5358.
(92) Ranaghan, M. J.; Schwall, C. T.; Alder, N. N.; Birge, R. R. Green Proteorhodopsin Reconstituted into Nanoscale Phospholipid Bilayers (Nanodiscs) as Photoactive Monomers. *J. Am. Chem. Soc.* **2011**, *133*, 18318−18327.
(93) Idso, M. N.; Baxter, N. R.; Narayanan, S.; Chang, E.; Fisher, J.; Chmelka, B. F.; Han, S. G. Proteorhodopsin Function Is Primarily Mediated by Oligomerization in Different Micellar Surfactant Solutions. *J. Phys. Chem. B* **2019**, *123*, 4180−4192.

https://doi.org/10.1021/acs.biomac.3c00034
Biomacromolecules 2023, 24, 1819−1838